Master's Thesis – Integrated Climate System Sciences

# SPARE-ICE Satellite Cloud Ice Retrievals

**Shengyin Li**

Matriculation number: 6517319

Born: 15th of June, 1990, in: Guangxi, PR. China

School of Integrated Climate System Sciences

University of Hamburg

Hamburg, 12 Nov. 2015

**Supervisor:**

Prof. Stefan Bühler

Dr. Verena Grützun

SPARE-ICE Satellite Cloud Ice Retrievals

This thesis has been accepted as a Master Thesis by the

Department Geowissenschaften der Universität Hamburg.

1. Reviewer: Prof. Stefan Bühler, Meteorology Institute

2. Reviewer: Dr. Verena Grützun, Meteorology Institute

# Contents

# List of Figures

# List of Tables

# Abstract

Ice Water Path (IWP) is an important quantity in climate research. To obtain the IWP data, which indicate the whole range of the ice cloud column, and also with long-term temporal range and large-scale spatial coverage, Holl et al. (2014) performed the cloud ice retrieval by employing the passive microwave and infrared remote sensing synergistically, and obtained a new IWP product: Synergistic Passive Atmospheric Retrieval Experiment-ICE (SPARE-ICE). Before being put into application, a validation of this new product is required. Based on the Artificial Neural Networks trained by Holl et al. (2014) with data of 2007 for IWP retrieval, this study processes more SPARE-ICE data of other years from 2006 to 2009, and aims at a comprehensive evaluation and validation of SPARE-ICE of these years.

A scene comparison is carried out involving IWP datasets like CMSAF (derived from AVHRR), MSPPS (derived from MHS), MODIS IWP, 2C-ICE and SPARE-ICE. Also, for the instantaneous field comparison of long-term data, SPARE-ICE is compared with 2C-ICE in depth to evaluate the retrieval algorithm; it is also compared with MODIS IWP, which is independent from SPARE-ICE retrieval. To gain insight of the potential application value of SPARE-ICE, the ECHAM model IWP dataset is also compared with SPARE-ICE. After collocation between IWP datasets, the simultaneous and spatial-coincident samples are obtained. With these collocated samples, the Linear Regression is used to identify their correlation. The Probability Density Functions (PDFs) are used to compare the IWP distribution. For observational and model data comparison, the Nash-Sutcliffe efficiency of the gridded monthly mean SPARE-ICE and ECHAM data is calculated. Besides, an Empirical Orthogonal Function (EOF) Analysis is performed to identify patterns in both datasets and highlight their similarities and differences.

The results show that SPARE-ICE not only displays the low value characteristics (lower than 500 $g/m^2$) as MODIS but also the high value characteristics (higher than 2500 $g/m^2$) approaching 2C-ICE. The collocated SPARE-ICE data are highly correlated with 2C-ICE data, with correlation coefficient of about 0.89 at low latitudes, and the performance of SPARE-ICE is not susceptible to cloud types. Although SPARE-ICE has less correlation (about 0.51) with MODIS, it is still satisfying. SPARE-ICE IWP distribution nearly coincides with 2C-ICE and MODIS without apparent bias. However, the performance of SPARE-ICE at low latitudes is better than at high latitudes. SPARE-ICE shows its potential value in model evaluation. It is a reliable and usable IWP product for climate research.

# 1 Introduction

## 1.1 Overview

Clouds play an important role in the radiation budget of the climate system. On one hand, they reflect incoming solar radiation, inducing a cooling effect on the Earth-Atmosphere system, and on the other hand they warm the Earth-Atmosphere system by absorbing outgoing long-wave radiation (IPCC, 2007). The net effect of clouds on the climate radiation budget is still an unresolved question. Clouds are the principal uncertainty source of this question (Charney et al., 1979). People generally divide clouds according to their altitudes and depthes to discuss this question. For example, the warming effect of high and thick clouds by the absorption of long-wave radiation is counteracted by their cooling effect caused by the reflection of short-wave radiation. However, high and thin clouds barely absorb and reflect short-wave incoming solar radiation, but absorb outgoing long-wave radiation. This contributes to a warming effect on the climate system.

Particularly, for ice clouds like cirrus, their net effect on the climate radiation budget is even more complex and difficult to identify. One additional reason is the strong scattering effect of the ice crystals, which is strongly dependent on the specific shape of the crystals. Apart from their effect on the climate radiation budget, ice clouds also influence the precipitation. Ice particles fall into lower level clouds and through the Wegener–Bergeron–Findeisen process (Wallace and Hobbs, 2006), which facilitate the attachment of ambient small water vapors, it triggers the Seeder-Feeder mechanism. As a result, growing particles will enhance the precipitation generation in lower clouds (e.g. Houze, 1994; cited from Buehler et al., 2007). Therefore, this study is interested in and will only focus on ice clouds and precipitating ice hydrometeors rather than liquid clouds. To investigate the net effect of ice clouds on the climate radiation budget, their radiative and optical properties should be determined first, and these two properties are closely related to the amount of ice water in the cloud (Eliasson, 2011).

An important quantity of ice clouds is the ice water path (IWP), defined as the mass of ice particles in the atmosphere above a unit surface area. It indicates the amount of ice in the air column (e.g., Wu, 1987). As an integrated quantity, it is easier to obtain IWP than ice profiles. IWP can, for example, be used to evaluate and improve the representation of ice cloud in climate models (e.g., Li et al., 2012), and to investigate aerosol-cloud interaction (e.g., Huang et al., 2006).

Practically, IWP is a quantity, for which the direct in-situ measurement is not achievable. In this case, satellite measurements become a common way for the acquirement of IWP data, hence also facilitate the investigation of the role of ice clouds in the climate system from a global scale and already for several decades (e.g., Schiffer and Rossow, 1983).

IWP data can be obtained by different satellite observation techniques, including infrared, visible light and microwave techniques. Eliasson et al. (2011) give an overview of the IWP relevant datasets and compares the observational results to climate models. However, electromagnetic waves of different frequencies are sensitive to different sizes of ice particles due to their attenuation (Buehler et al., 2007), as a result, they detect different parts of the cloud column. Therefore, the IWP values obtained from different frequency sensors show significant disagreement (Waliser et al., 2009; cited in Eliasson et al., 2013). Eliasson et al. (2013) compares different IWP datasets based on the collocation toolkit developed by Holl et al. (2010). The conclusions of the comparisons are corresponding to the nature of each technique. For example, infrared sensor alone can only obtain IWP from thin cirrus. For more detailed discussion of the advantages and limitations of each technique, please refer to Section 1.2. Additionally, Eliasson et al. (in preparation) discussed the uncertainty of MODIS IWP retrieval on account of cloud scenario.

Space-borne cloud RADARs and LIDARs, as active microwave remote sensing techniques, are into exploitation in recent years. The combination of RADAR and LIDAR techniques provides relatively more accurate IWP information than passive remote sensing, especially, they also see the profile of cloud ice.

To acquire the IWP dataset, which has the value that indicates the whole range of the ice cloud column, and also with long-term temporal and large scale spatial coverage, Holl et al. (2014) performed the cloud ice retrieval (Synergistic Passive Atmospheric Retrieval Experiment-ICE, SPARE-ICE) by training the Artificial Neural Networks (ANN), based on the synergy of both infrared and passive microwave techniques. This progress takes advantage of both, passive remote sensing (as the data used for retrieval) and active remote sensing (as the reference for retrieval), meanwhile compensates their respective limitations.

Since many data centers still lack accurate and long term IWP data, SPARE-ICE as a new IWP product could be provided to the community, for example, via the CliSAP-Integrated Climate Data Center in the future. Before that, the validation of this new product is necessary. In terms of validation, Holl et al. (2014) conducted a simple comparison between SPARE-ICE and 2C-ICE with the data of 2007. The

2C-ICE dataset of 2007 is the retrieval reference in the training of ANN, hence is not independent with the retrieval itself. Therefore, this comparison is not sufficient for the SPARE-ICE validation.

In this study, apart from the reference dataset 2C-ICE of years other than 2007 will be compared to examine the performance of the neural network, the independent datasets MODIS IWP will also be involved in the comparison. Additionally, to have a glance of the rationality and application prospect of SPARE-ICE, this study will compare the climate model ECHAM data with SPARE-ICE .

In the following context, Section 1.2 will give an overview of satellite remote sensing and IWP retrieval principle for several techniques; Section 2 will introduce the SPARE-ICE dataset and its underlying datasets, as well as the required Artificial Neural Network technique for the development of SPARE-ICE (Holl et al. 2014); Section 3 will introduce the other IWP datasets for the evaluation and validation of SPARE-ICE. Section 4 will illustrate the collocation method (Holl et al. 2010), which is commonly used to process the paired datasets before comparison in this study, and also some statistical methods for data comparison; Section 5 will present the results of the comparisons between SPARE-ICE and other datasets with some conclusive or speculative discussions; Section 5 will conclude the reliability of SPARE-ICE.

## 1.2 Background Knowledge

To understand the disagreements of different datasets on IWP values, this section introduces principles of different remote sensing techniques. For different techniques, IWP values are derived by exploiting the absorption, reflection and scattering effects of cloud ice particles on electromagnetic waves.

At a specific wavelength, the optical depth indicates how much electromagnetic wave can penetrate through the cloud. Many techniques attempt to derive the ice cloud optical depth and the cloud ice particle effective radius, and subsequently, derive IWP value based on the fact that the IWP value is proportional to the ice cloud optical depth and cloud ice particle effective radius (Holl, 2011).

Remote sensing generally can be divided into active remote sensing and passive remote sensing. Accordingly, satellite sensors can be divided into two categories: passive sensors and active sensors. Active remote sensors, like RADAR and LIDAR, receive the electromagnetic wave initially emitted by themselves and back-scattered by the particles in the atmosphere. Passive sensors, including infrared (IR), visible

light (VIS) and passive microwave (PMW) sensors on the satellite, detect the energy, which is originally coming from the solar radiation or the terrestrial infrared and microwave radiation. Figure 1 is the radiation spectrum range from Ultra-Violet to IR band.

### 1.2.1 Passive Remote Sensing

Satellite VIS (390 nm to 700 nm, or 430 THz to 790 THz) channels measure the solar reflectance of the Earth surface and cloud top. IR (700 nm to 1 mm, or 430 THz to 300 GHz) and Passive Microwave (PMW) (1 mm to 1 m, or 0.3 GHz to 300 GHz) channels can be divided into sounding channels and atmospheric window channels. IR and microwave radiation can be absorbed by the atmospheric components like water vapor, as shown in Figure 1. The channels, which exploit the absorption of radiation

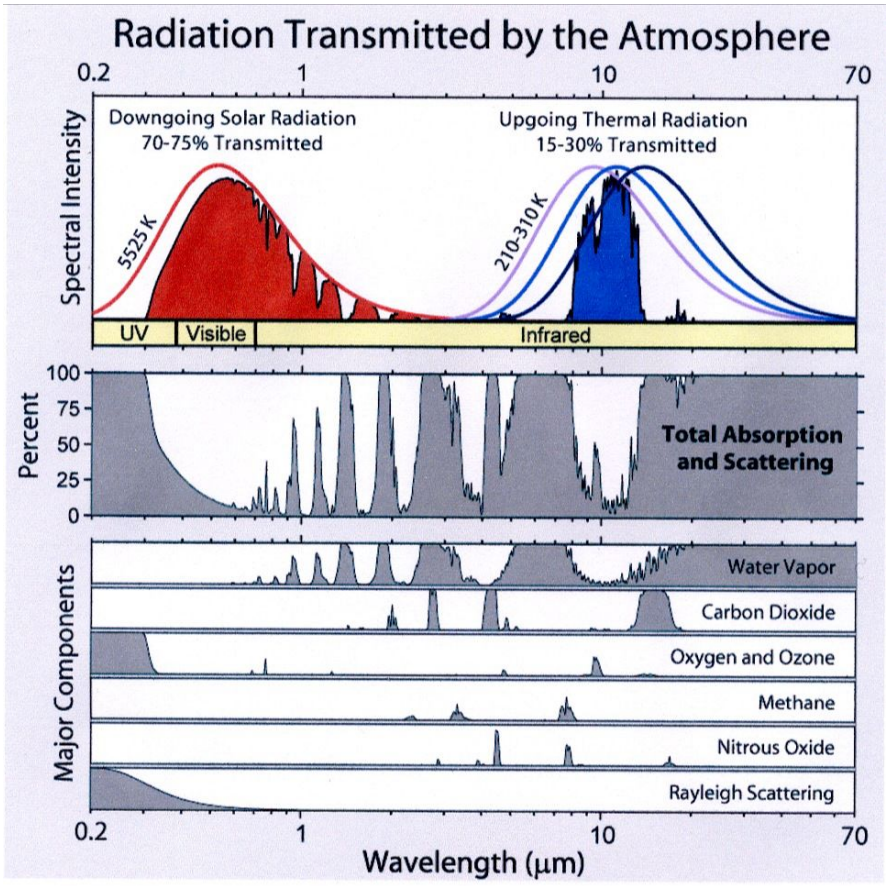


Figure 1. Radiation Spectrum of the Atmosphere (Figure by Robert A. Rohde, taken from open access source: Wikipedia http://en.wikipedia.org/wiki/Absorption_band 25 August 2007)

by water vapor, are called water vapor channels. There are also other species causing absorption, but in my study, the relevant sounding channels are water vapor channels.

For the water vapor channel (for example, around 7 μm in Figure 1), the electromagnetic wave is sensitive to the water vapor. According to Kirchhoff Law, if the water vapor absorbs the electromagnetic wave in a specific wavelength, then it will emit the electromagnetic wave in the same wavelength. A good absorber is also a good emitter. The satellite only receives the energy emitted by the water vapor, which absorbs the upwelling radiation emitted by the Earth surface and low clouds. In other words, the Earth surface below the water vapor is normally not visible. The atmosphere is opaque for the satellite at these wavelengths. The satellite receives lower thermal radiance from water vapor, which located at a higher altitude compared to the Earth surface. It is worthwhile to note that, the sounding channels are also able to detect the Earth surface when the atmosphere is in relatively dry condition.

In some of the other ranges of the spectrum (for example, around 2.5 μm in Figure 1), the radiation is not absorbed by any atmospheric components. These ranges are called atmospheric windows. Channels in the atmospheric window region are called surface sensitive channels or atmospheric window channels. They are sensitive to the Earth surface. In other words, the atmosphere is transparent for the radiation. Therefore, the window channels are used to detect the Earth surface.

IR channels alone can only detect thin (but not too thin) clouds like cirrus (Buehler at al., 2007). Thin clouds can be seen by satellite IR channels because of their semi-transparent characteristics. Due to the high altitude compared to the Earth surface, the brightness temperature of semi-transparent clouds is lower than the Earth surface. The contrast of brightness temperature between the cloud and the Earth surface is used to derive IWP. For a thick cloud acting like a black body, only the thermal emission of the cloud top can be seen by satellite IR channels, and therefore IWP cannot be retrieved in that case.

Combining IR and VIS techniques together, IWP can be obtained by using the Solar Reflectance Bispectrum (SRBS) method (Nakajima and King, 1990; cited from Eliasson et al., 2013). In the SRBS method, the solar reflectances of one pair of cloud reflection measurements (one VIS or Near IR channel, and one thermal IR channel) are recorded into a look-up table. From this look-up table, the cloud optical depth and ice particle mean effective radius are retrieved simultaneously. Subsequently, IWP can be obtained, because it is a function of ice effective radius and cloud optical depth. In this method, both IR and VIS techniques work collaboratively. Nevertheless, this method can only be used for daytime IWP retrieval, because it involves solar channels.

Besides, for a thick cloud, the reflection of solar radiation only happens at its upper part. Therefore, this method is restricted to thin clouds or the upper part of thick clouds.

Passive microwave technique for deriving IWP is based on the water vapor channels in the microwave bands. The ratio of particle size and electromagnetic wavelength of the electromagnetic wave determines what kind of interaction happens on the particle. For large ice particles, the interaction with microwave is scattering. This scattering effect, rather than the low thermal emission, accounts for the reduction of radiance received by microwave channels. The water vapor channels are able to obtain the IWC profile by the depression of brightness temperature compared to no cloud cases (Buehler et al., 2007). Microwave observations are more sensitive to large particles and strongly penetrate clouds, so that they are able to detect large ice particles in lower parts of the cloud.

### 1.2.2 Active Remote Sensing

In general, RADARs detect clouds based on the back-scattering effect of cloud droplets, ice crystals and etc. to the radio wave. It measures how much back-scattering energy from the originally transmitted electromagnetic wave goes back to the RADAR antenna after interacting with the cloud target. To describe the size distribution of cloud hydrometeors, RADAR Reflectivity is a quantity defined as a function of the sixth power of particle diameter under the condition that particle diameter is much smaller than the wavelength of the radiation (Rayleigh-scattering). When the situation doesn't meet this condition, measurements obtain the Equivalent RADAR Reflectivity ($Z_E$). In early researches of deriving IWC from $Z_E$, there is generally a IWC-$Z_E$ relationship from ice particle size spectra (e.g., Heymsfield, 1977). IWC, and also IWP can be acquired from this IWC-$Z_E$ relationship. However, this relationship can be employed only under a particle size distribution assumption. The high frequency RADAR is able to measure deep inside clouds. The RADAR wave transmitted by a microwave RADAR, e.g. a 94 GHz RADAR, is sensitive to large particles.

LIDAR emits the laser beam, and then also measures the backscattering energy of the cloud object going back to the LIDAR telescope. The extent of the laser beam attenuation is determined by scattering properties of particles to the laser. This effect is indicated by the cloud and aerosol extinction coefficient, which is an indicator of the cloud optical depth, and hence link to the cloud water path. For a polarization

LIDAR, its polarization capability allows the LIDAR to detect the shape of particles as well as their phases. Nevertheless, due to the strong attenuation of the laser beam, LIDAR only detect the top of the cloud, where only small ice particles exist. In recent years, the LIDAR technique is combined with RADAR technique to derive more accurate IWP than derived from RADAR or LIDAR alone.

For active sensors, the retrieved Ice Water Content (IWC) is strongly dependent on the assumption of particle size distribution (Deng et al., 2010; cited from Holl et al., 2014). This factor due to its contribution to the uncertainty of the IWP retrieval, however, can be attributed to one of their limitations. Another limitation is the high expense of active system on-board satellite. This study employs only active sensors, which are on-board a satellite.

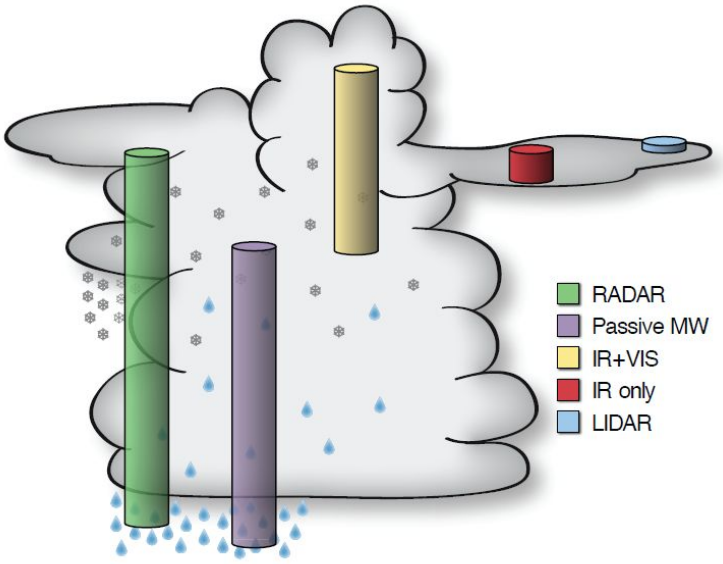


Figure 2. Schematic of the sensitive part in the cloud column for different remote sensing techniques. Adapted from “Assessing observed and modelled spatial distributions of ice water path using satellite data” by S. Eliasson et al., 2011, Atmospheric Chemistry and Physics, 11(1), P380. Copyright 2011 by S. Eliasson. Adapted with permission.

Figure 2 depicts that which part of the cloud column each technique described above is sensitive to. We can see from that, the combined RADAR and LIDAR technique is able to detect the whole range of the cloud column. Besides, it is worthwhile to note that combining Passive MW, IR and VIS techniques is also able to detect the whole range of the cloud column.

# 2 SPARE-ICE

SPARE-ICE is an IWP product developed by Holl et al. (2014) using Artificial Neural Networks (ANN) with data from passive sensors: the Advanced Very High Resolution Radiometer (AVHRR) and the Microwave Humidity Sounder (MHS). Firstly, as mentioned in last section that the combined Passive MW, IR and VIS technique is able to detect the whole cloud column, but there is still no such an IWP product. That is the reason why the data of passive sensors AVHRR and MHS are chosen to develop SPARE-ICE for IWP data with a large spatial and temporal range. Secondly, since the combined RADAR and LIDAR technique is also able to detect the whole cloud column, an existing IWP product, the combined RADAR and LIDAR dataset 2C-ICE, is chosen as the reference for training the ANN. ANN is an efficient and convenient method to extract nonlinear relations between the passive sensors data and active sensors data. Therefore, it is employed for IWP retrieval. This section introduces sensors and datasets relevant to retrieve SPARE-ICE IWP, and the ANNs for SPARE-ICE development, as well as the new SPARE-ICE data processing.

## 2.1 Underlying Sensors and Datasets

### 2.1.1 AVHRR and MHS

AVHRR is a sensor with infrared and solar channels carried on the Polar Orbiting Environment Satellites (POES) launched by National Oceanic and Atmospheric Administration (NOAA) in 1978 (Price, 1984), and on the MetOp launched by EUMETSAT in 2006 (Albiñana et al. 2007). The resolution of AVHRR data is about 1 km at nadir.

The Advanced Microwave Sounding Unit B (AMSU-B) is on-board POES of NOAA15 since 1998, and of NOAA-16, and -17 subsequently (Kleespies et al., 2006). Another passive microwave sensor MHS, is the improvement of AMSU-B. It functions similarly as AMSU-B and took place of it in 2005 from NOAA-18, -19, MetOp-A, and MetOp-B on. MHS has 5 channels ranging from 89 GHz to 190 GHz. Two channels at 90 GHz and 157 GHz (channel 1 and 2) are surface sensitive channels. Three channels at 183±1 GHz, 183±3 GHz and 190 GHz are water vapor channels. The footprint radius of MHS/AMSU-B is approximately 16 km at the nadir.

AVHRR and MHS/AMSU-B have the same platforms (on-board both POES of NOAA and MetOp of EUMETSAT). The swath width of MHS/AMSU-B is about 2348 km, and the swath width of AVHRR is about 2600 km. These two datasets are used as inputs in the retrieval of SPARE-ICE IWP because of their large temporal and spatial coverage.

### 2.1.2 2C-ICE

The Cloud Profiling Radar (CPR) is a space-borne microwave weather RADAR on-board satellite CloudSat. CPR, which operates at 94GHz, provides the vertical profile of Ice Water Content (IWC) in a vertical resolution of 250m. IWP is the vertical integral of IWC. The Cloud-Aerosol Lidar with Orthogonal Polarization (CALIOP) is a two-wavelength polarization LIDAR on-board the satellite Cloud-Aerosol Lidar and Infrared Pathfinder Satellite observation (CALIPSO) (Winker, 2009).

2C-ICE is the level 2 product of CloudSat. The IWP of 2C-ICE is derived from both CALIOP and CPR data (Mace and Deng, 2011). A similar dataset is Active combined raDAR-liDAR product (DARDAR), which is also an IWP product based on the combination of CALIOP and CPR. Both datasets cover the whole range of IWP values in other datasets, and have very high similarities. To choose 2C-ICE was a spontaneous decision by Holl et al. (2014) and it was kept in my study subsequently.

However, 2C-ICE has limited spatial coverage (about 1.4 km swath width) due to the narrow swath of CPR and CALIOP. Also, CPR and CALIOP can only provide data of recent years (since 2006). This makes 2C-ICE unsuitable for long term climate research.

## 2.2 Artificial Neural Network

Holl et al. (2014) developed SPARE-ICE by training the Artificial Neural Networks (ANNs). An ANN generally contains many neurons (nodes) as processing units. These nodes are distributed into three layers. The first layer is the input layer and the last layer is the output layer. The intermediate layer between the input and output layer is the hidden layer. The output is compared to the target dataset, which is also called the reference of ANN. The random weights (denoted by $W_1$ to $W_n$) and biases (denoted by $b_1$ to $b_n$) are assigned to inputs at the beginning. The activation function can be expressed as

$$A = \phi\left(\sum_{i=0}^{n}(X_i W_i + b_i)\right), \qquad \text{(Equation-1)}$$

where $\phi$ represents for the non-linear function.

To minimize the difference between the outputs and the targets, ANN is trained by adjusting the weights and the biases iteratively. This is the learning process of the neural network. Figure 3 illustrates the general ANN working principle. For more basics of the general ANN and its geophysical applications, please refer to e.g. Krasnopolsky (2007).

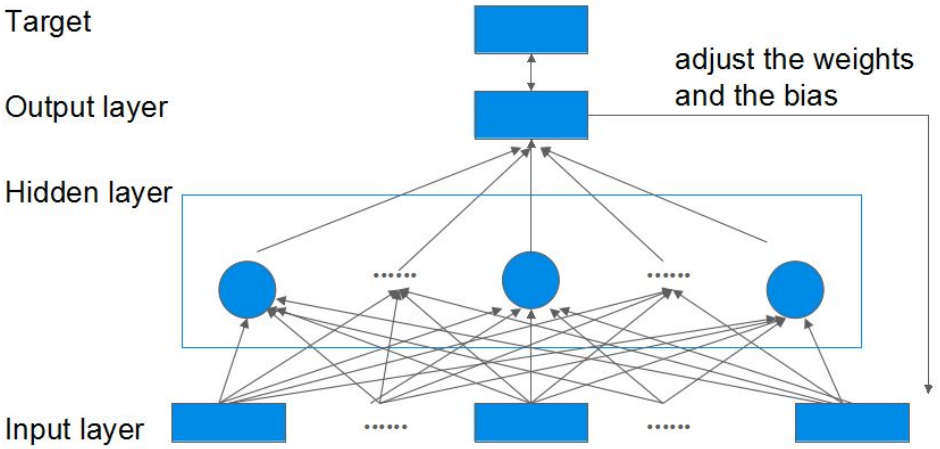


Figure 3. Illustration of the Artificial Neural Network

In this study, the ANN being utilized is a Feed-Forward Network with 10 neurons at only one hidden layer. To perform the SPARE-ICE retrieval, Holl et al. (2014) separates the whole process into three stages: firstly developing the artificial neural networks, secondly evaluating their performances, finally employing the optimal ones to process IWP data.

More specifically, during the development of neural networks, Holl et al. (2014) trained a pair of neural networks with the data of 2007: one is for cloud detection; another is for IWP retrieval. The cloud detection neural network aims at identifying the cloud percentages, and later will be used as cloud filter, in case of for example, misidentifying snow cover as cloud ice. The IWP retrieval neural network is used to derive IWP in log scale, because IWP tends to be a log-normal distribution.

During the development, the inputs of the ANN are the collocated data from the selective IR and solar channels of the AVHRR, the water vapor channels of the microwave sensor MHS and the auxiliary information like the viewing angle of the sensors and surface elevation. As mentioned above, 2C-ICE covers the whole range of IWP values in other datasets. Therefore, it is used as the target dataset.

Before the development of SPARE-ICE, the collocated datasets are divided into three categories: training data, validating data and testing data. The training data are used for minimizing the difference between the output and the target. However, ANN not only learns the relationship between inputs and targets, it also learns the relationship between inputs and targets. This phenomenon is called ‘overfitting’. To control this problem, the second category of data, the validating data, are used for stopping the training process in case of ‘overfitting’. When the outputs tend to fit the targets but start increasing the differences to the validating data, the ANN stops the iterative process. If this doesn’t happen, the ANN will stop after five iterations. The testing data are independent from the training process. Therefore, they are used for the evaluation of the performance of ANNs.

Afterward, the performances of the ANN was evaluated by comparing with other ANNs with different configurations, for example, with or without solar channels. When one pair of artificial neural networks with optimal performance is obtained, it will be employed in the IWP retrieval for data of other years. The infrared channels of AVHRR, the water vapor channels of MHS, and the auxiliary information including the local zenith angle, the local azimuth angle and the surface elevation are employed in the final ANN to retrieve IWP.

The evaluation of artificial neural networks shows that, including or excluding solar channels, the results only marginally differed. Therefore, the SPARE-ICE retrieval was done without solar channels. That means SPARE-ICE is able to provide not only daytime IWP data, but also nighttime IWP data. This is an advantage compared to other IWP datasets derived by VIS+IR techniques. However, in this case, for the sake of data consistency, when evaluating the performance of artificial neural networks with respect to with or without solar channels in Holl et al. (2014), IWP was retrieved from the same data. That is to say, only the day-time data are included in both neural networks, and this is conducted by the restriction of solar zenith angle. I kept the restriction of solar zenith angle as Holl et al. (2014), because the performance of night-time data haven’t actually been evaluated. Therefore, although the solar channels of AVHRR are not employed, and SPARE-ICE should be able to provide day and nigh data in principle, SPARE-ICE doesn't show night-time data in my study. As shown in Figure 4, the SPARE-ICE data have no value in Arctic in January.

The SPARE-ICE retrieval is based on the combination of MHS and AVHRR. Although the inherited horizontal resolution from MHS is lower compared to CPR and CALIOP, most importantly, the temporal (since 1999) and spatial coverage (about 2348 km swath width) of MHS/AMSU-B and AVHRR are much higher than 2C-ICE. However, 2C-ICE is an ideal reference for the SPARE-ICE retrieval for the sake of its relatively accurate IWP value, which indicating the whole range of cloud column. Therefore, SPARE-ICE retrieval is very useful for exploiting the advantages of both passive and active datasets.

## 2.3 SPARE-ICE Data Processing

Holl et al. (2014) have already processed the data of 2007 and 2013. To process more SPARE-ICE data of other years, I applied the Artificial Neural Networks developed by Holl et al. (2014) directly and kept all of its original configurations, as this pair of ANNs had been evaluated and tested, and functions best.

The input data for the retrieval are prepared. They include the collocated MHS and AVHRR data. Note that, although AVHRR and MHS are on-board the same platform, the reason for their collocation is due to their footprint size difference. Additionally, the surface temperature data (from 2006 June to 2010 June) extracted from NCEP Climate Forecast System Reanalysis (CFSR) data (Saha et al., 2010) are also used in the procedure of SPARE-ICE data processing, but only used for cloud detection, not for retrieve IWP data.

MHS on-board NOAA18 and NOAA19 have larger number of occurrences for collocation with CloudSat than on-board other NOAA series (Holl et al., 2010), hence, I chose the data of MHS and AVHRR on-board NOAA18 to process new IWP data. Another reason for choosing NOAA18 is that the training of ANN for IWP retrieval by Holl et al. (2014) was based on the data from NOAA18. To ensure the consistency of satellite platform for the new IWP data, I kept the choice of NOAA18 as before.

The SPARE-ICE data I processed are from 2006 June to 2010 July (except 2007, which were processed by Holl et al., (2014)), hence this study has four consecutive years of SPARE-ICE data available. Table 1 summarizes the temporal range of the data used in this study.

Figure 4 shows the new processed SPARE-ICE data and the 2C-ICE data on Juanuary 11$^{th}$ of 2008 from a global view. We can see that wide tracks of SPARE-ICE one day data cover almost the whole Earth, while narrow tracks of 2C-ICE have very

limited spatial coverage. High IWP values distribute in three zones: ITCZ and westerlies in Northern Hemisphere and Southern Hemisphere. Clouds in these regions extend to very high altitudes where the cloud ice formation happens. Overall, in the ITCZ region, IWP values are higher than in other regions.

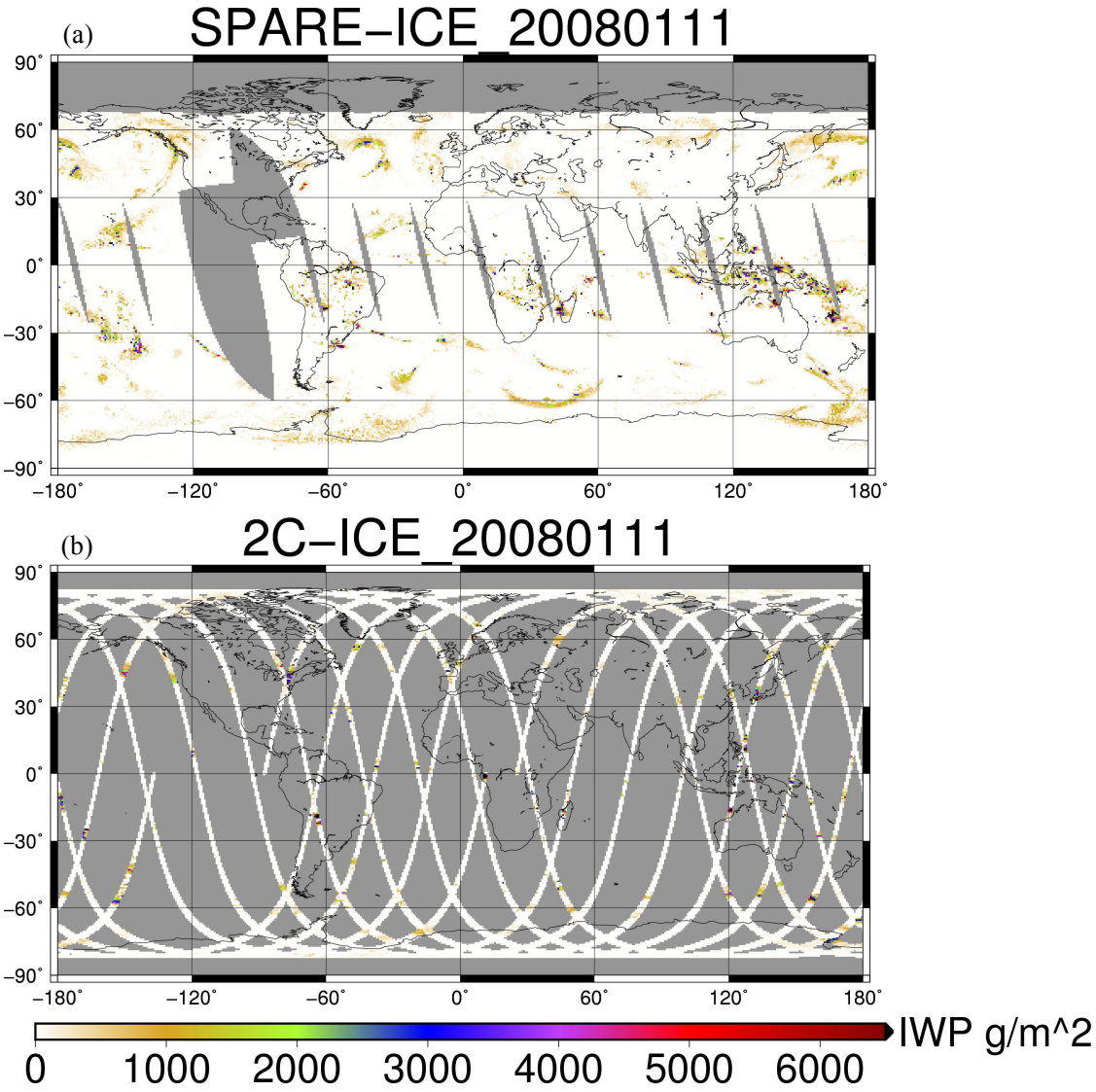


Figure 4. A global view of SPARE-ICE IWP data (a) and 2C-ICE IWP data (b), on Jan. 11th, 2008 (without collocation).

Table 1. Time period of the processed data and of validation

| | Time period |
|---|---|
| SPARE-ICE data processing | 2006 Jun. - 2010 Jul. (except 2007, which is processed by Holl et al.,2014) |
| SPARE-ICE v.s. 2C-ICE | 2008 |
| SPARE-ICE v.s. MODIS | 2008 Jan. 11$^{th}$ |
| SPARE-ICE v.s. ECHAM | 2007 - 2008 |

# 3 Datasets for Comparison

## 3.1 Observational Datasets

The Moderate Resolution Imaging Spectroradiometer (MODIS) (Yang et al., 2006) is a sensor on-board satellite Terra and satellite Aqua. In this research, I use MODIS data acquired from Aqua, collection 6. MODIS has both solar and infrared channels as AVHRR. The resolution of MODIS is about 1 km. Passive combined IR and VIS techniques are sensitive to very small particles. For example, some channels of MODIS with the wavelength around 10 μm are sensitive to particles of a diameter within 100 μm (Buehler et al., 2007). MODIS cannot detect the deeper part of the cloud, it makes judgment about the whole cloud phase based on the cloud top; hence, it tends to overestimate IWP for the mixed-phased clouds, which have liquid water content (LWC) rather than IWC at the lower part of clouds. Eliasson et al. (in an internal study) discussed this problem and also proved that for MODIS collection 5.1, this phenomenon is very apparent. Nevertheless, the error from this problem is reduced in collection 6. That is why I use the MODIS data of collection 6 in this study.

The Satellite Application Facility on Climate Monitoring (CMSAF) uses AVHRR data to derive IWP data. The IWP data is directly available in the CMSAF dataset. This product combines four original footprints of AVHRR, hence it is resolution is 4 km × 1 km.

The operational Microwave Surface and Precipitation Products System (MSPPS) is a passive microwave product providing the IWP derived from AMSU-B/MHS (Holl et al., 2014). The resolution of MSPPS is about 16 km inherited from the footprint size of MHS.

2C-ICE data will be first used in the scene comparison, as the representation of active sensor dataset, and latter used in the precise comparison with a whole year data of 2008. For the relevant introduction of 2C-ICE, please refer to Section 2.1.2.

Table 2 summarizes the main information of IWP-relevant datasets derived from sensors introduced above. For different sensors, their footprint sizes on the Earth surface change with their viewing angles. The smallest footprint is at nadir. For this reason, only the spatial resolution at nadir is shown in Table 2. For more description on IWP relevant sensors and datasets, please refer to the thesis by Eliasson (2011).

Table 2. Key information of observational IWP datasets

| Dataset/Product | Satellite/Instrument | Spectrum | Spatial Resolution at nadir |
|---|---|---|---|
| CMSAF | AVHRR | VIS, IR | 4 × 1 km |
| MODIS/ MYD06_L2 | MODIS | VIS, IR | 1 × 1 km |
| MSPPS | MHS or AMSU-B | MW (passive) | 15 km at the nadir |
| 2C-ICE | CloudSat/CPR & CALIPSO/CALIOP | MW (active) | Horizontal 1.1× 1.1 km |
| DARDAR | CloudSat/CPR & CALIPSO/CALIOP | MW (active) | |
| SPARE-ICE | MHS + AVHRR | MW + IR | Footprint diameter of 15 km |

CMSAF, MODIS, MSPPS and 2C-ICE will be utilized for the scene comparisons with SPARE-ICE in Section 5.1.

For the further precise comparisons of long-term data, 2C-ICE data of 2008 will be used to evaluate the performance of the neural network development; MODIS, as an independent dataset from SPARE-ICE, will be also involved in the validation of SPARE-ICE.

SPARE-ICE is further compared with 2C-ICE by specifying cloud type samples. The cloud type information are acquired from the combined CloudSat/CPR and CALIPSO/CALIOP cloud classification product 2B-CLDCLASS-LIDAR. Although, compared to passive cloud type classification, active cloud type classification has the advantage of detailed information on cloud vertical profile and more accurate cloud phase, but it still has many limitations (Sassen and Wang, 2008). For example, the horizontal scale estimation of cloud is not possible due the limited spatial coverage of both the relevant active sensors. Hence the confidence level of this cloud type product remains disputed. However, it is convenient to use this product, since it is from the same sensors as 2C-ICE.

## 3.2 Model Dataset: ECHAM

For the application aspect, to gain insight of SPARE-ICE used for model evaluation, I compare it with ECHAM model (MPI-ESM-LR) (Stevens et al., 2013). ECHAM is an atmospheric general circulation model, developed at the Max Planck Institute for Meteorology. “EC” is a short form of European Centre for Medium-Range Weather Forecasts (ECMWF), and “HAM” is a short form of “HAMBURG”, where it is developed. One of the ECHAM output variables is IWP. The available ECHAM IWP data range from 1979 till 2008, with the 192 × 96 global grids. In my study, the data I downloaded are the daily data of ECHAM version 6, AMIP experiment, and CMIP5 project. However, the IWP defined by ECHAM is not the same as my context. It describes the mass of cloud ice in the cloud column, which is in model grid size, divided by the area of the whole grid size, rather than the cloud area. To calculate the IWP in our concept, the IWP of ECHAM has been divided by the total cloud fraction, which is another variable of ECHAM.

# 4 Method

## 4.1 Collocation Method

To make the precise comparison of two datasets from different satellite sensors feasible, the collocation is a process to search for footprints of two sensors sweeping over almost the same location nearly simultaneously. This process is always conducted by specifying both temporal and spatial thresholds, within which the footprints can be regarded as collocated. The collocation toolkit developed by Holl et al. (2010) is able to search for footprints of two datasets within specified thresholds. For the details of the collocation algorithm, please refer to Holl et al. (2010).

According to the temporal and spatial variation of clouds, the collocation thresholds should not be too large; otherwise the target will be not consistent. Based on the footprint sizes of sensors, one can specify, for example, the radius of the large footprint as the spatial threshold. After that, the temporal threshold can be determined roughly by the estimated wind speed at high altitudes. Note that, if the distance threshold is defined as the footprint radius at nadir, some collocations might be lost, because the real size of the footprint on the earth surface changes with satellite viewing angles. Some MHS footprints, which are much out of nadir, cover more CPR footprints. In my study, for example, the temporal thresholds for the collocation between SPARE-ICE and 2C-ICE and collocation between SPARE-ICE and MODIS are both 600 s; the spatial thresholds are both 7.5 km. For more details on any collocations conducted in this study, please refer to Table 3.

The number of collocations varies with latitudes, viewing angles, time of day and day of month (Holl et al. 2010). For example, in high latitudes, there are more collocations, because from the same size of surface area, CloudSat obtains more samples in high latitudes than in low latitudes. Sensors like CloudSat/CPR and CALIPSO/CALIOP flying in the A-Train satellite constellation have more ground tracks overlapping with sensors on-board NOAA18 and Aqua, because they both are also near to A-train (Holl et al., 2010; Stephens et al., 2002). NOAA 18 and NOAA 19 have highest collocation occurrence number with CloudSat/CPR (Holl et al., 2010). Therefore, in this study, I use the collocations between MHS and AVHRR on-board NOAA 18.

If the two collocated datasets have large differences in footprint size, many small footprints are within one large footprint. Hence, there would be many collocations for

the same large footprint, as illustrated in Figure 5. IWP values of small footprints are 'collapsed' to one large footprint by calculating their average. Concerning the sampling effect, as described by Holl et al. (2010), in the subsequent comparison of two collocated datasets, the standard deviation of the small footprint IWP within one large footprint and the number of collocated small footprints within one large footprint are also calculated as thresholds to discard same collocations, which are not representative due to too few overlap area or too large spatial variation within one large footprint.

Table 3. Criteria for reading the collocated data

| Figure ID | Objects | | Distance (km) | Time interval (s) | Latitude (degree) | No. of small footprints | Cloud filter |
|---|---|---|---|---|---|---|---|
| Figure 9 (a) | SPARE-ICE | 2C-ICE | 7.5 | 600 | [-90 90] | >=10 | Fract10 =100% |
| Figure 9 (b) | SPARE-ICE | 2C-ICE | 7.5 | 600 | [-30 30] | >=10 | Fract10 =100% |
| Figure 11 | SPARE-ICE | 2C-ICE | 7.5 | 600 | [-30 30] | >=10 | |
| Figure 16 | SPARE-ICE | MODIS | 7.5 | 900 | [-90 90] | | |

* 'Fract10 =100%' means: if IWP value of the secondary footprint is larger than 10 g/m$^2$, this sample counts as cloud; and within one large footprint, the cloudy secondary footprints account for 100%.

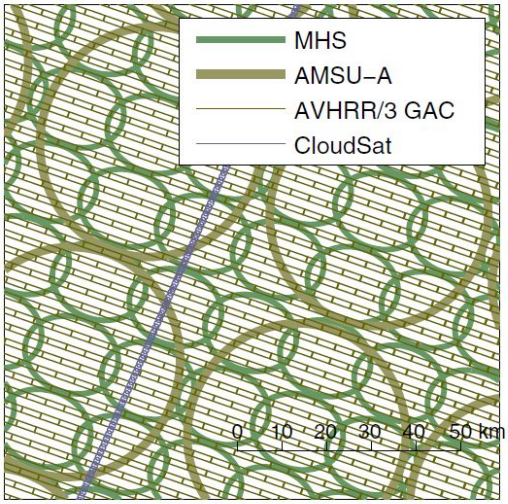


Figure 5. Illustration of footprints from different datasets. Adapted from “Systematic and random errors between collocated satellite ice water path observations” by S. Eliasson et al., 2013, Journal of Geophysical Research: Atmospheres, 118(6), P2634. Copyright 2013 by S. Eliasson. Adapted with permission.

## 4.2 Comparison Scheme and Data Post-Processing

To evaluate and validate SPARE-ICE systemically, I first compare SPARE-ICE IWP with 2C-ICE, which is the ANN reference; secondly, I compare it with MODIS, which is an independent dataset in the SPARE-ICE IWP deriving stage; at the end, to see its potential application, I compare it with ECHAM model. Figure 6 demonstrates the relationships between SPARE-ICE and the datasets used for SPARE-ICE validation. Apart from the datasets mentioned above, Figure 6 additionally demonstrates a ground-based IWP dataset Jülich ObservatorY for Cloud Evolution (JOYCE) as an example of the cloud observation from a ground site. A complete and comprehensive validation of satellite data is often done by comparing with ground-based data. Although JOYCE is not from an in-situ measurement, it is still a appropriate dataset as the comparison reference in the validation of SPARE-ICE. However, it is not used in this study because of lacking the temporal overlapped data with the processed SPARE-ICE data.

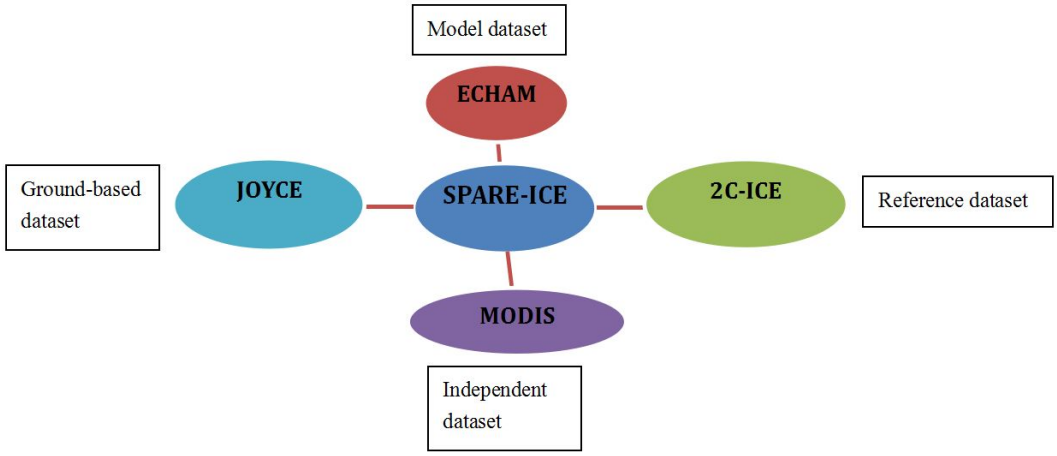


Figure 6. Diagram of the relationships between the comparative datasets

The instantaneous field comparison includes scene comparison in Section 5.1 and the comparisons based on the long-term collocated data samples. Scene comparison is a comparison by eye for case study by selecting a scene at a specific time with a strong and long-lasting weather system with high IWP values. For different datasets, the same scene within several minutes till several hours will be shown, and the comparisons can be conducted directly by bare eyes. This approach compares the original data from all datasets unsimultaneously, and gives us a first quantitative view on the results.

The instantaneous comparison with long-term data between SPARE-ICE and 2C-ICE is based on their collocated data of 2008. For the comparison with specific cloud type samples, the collocations between SPARE-ICE and 2C-ICE are further collocated with the combined CloudSat CPR and CALIPSO CALIOP cloud classification product 2B-CLDCLASS-LIDAR. The averaged field comparison is conducted by regridding and averaging of SPARE-ICE and 2C-ICE data. Because of the limited spatial coverage of 2C-ICE, the averages exclude the missing values (NaN), which come from the region that CloudSat doesn't sweep over. More specific details, like collocation criteria, for all collocations in this study, are shown in Table 3.

Due to the high resolution and wide coverage of MODIS, the MODIS and SPARE-ICE collocation collects much more spatial and temporal coincident samples than the 2C-ICE and SPARE-ICE collocation (the number of one year of 2C-ICE and SPARE-ICE collocation occurrence is comparable to the number of one day of MODIS and SPARE-ICE collocation occurrence). The MODIS and SPARE-ICE collocation requires much longer running time. Therefore, I only collocated one day of MODIS and SPARE-ICE data in this study.

The overlap temporal range of available processed SPARE-ICE and ECHAM is from 2007 to 2008. For averaged field comparison between SPARE-ICE and ECHAM, I regrid SPARE-ICE data to the grid size of ECHAM. Figure 7 shows the main procedure of all data processing in this study, including some details of technical process. Also, as mentioned before, the IWP of ECHAM has been divided by the total cloud fraction.

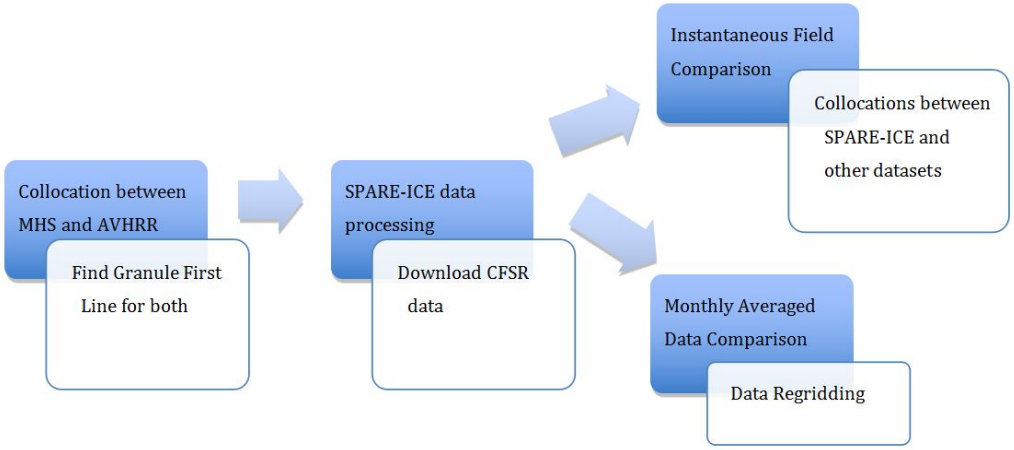


Figure 7. Flow chart of data processing

## 4.3 Statistical Methods for Evaluation

With the collocated data, the Fractional Error (FE) is defined after Holl et al. (2014) as

$$FE = \exp\left|In\frac{IWP_{\text{Retrieval}}}{IWP_{\text{Reference}}}\right| - 1 \qquad \text{(Equation-2)}$$

and is an indicator of the SPARE-ICE performance defined by Holl et al. (2014). $IWP_{Retrieval}$ means the resultant IWP value from the retrieval; $IWP_{Reference}$ means the reference for comparison. In our case, $IWP_{Retrieved}$ denotes SPARE-ICE data, and $IWP_{Reference}$ denotes 2C-ICE data. In the following context, "MFE" a short form of "Median of Fractional Error". FE expresses the error of SPARE-ICE referring to 2C-ICE, particularly since SPARE-ICE is derived from a log-normal scale. In our case, an ordinary difference is not mathematically meaningful for data on a log-normal scale.

To demonstrate, if two comparative IWP values are 50 g/m$^2$ for the retrieval and 200 g/m$^2$ for the reference, or the other way around, the corresponding FE is 300%; if

the IWP values are 50 g/m$^2$ for the retrieval and 100 g/m$^2$ for the reference, or the other way around the corresponding FE is 100%. For the comparison of two groups of IWP data, the Median of Fractional Errors (MFE) are generally calculated in both Holl et al. (2014) and this study.

The Linear Regression of the collocated datasets is carried out to obtain the correlation coefficients between SPARE-ICE IWP and the other IWP datasets. It indicates how well they correlate with each other. It is seen in the scatter plot and indicated by the loose or compact distribution of scattered points.

Similar to the concept of scatter plot, a quantity, named scatter, quantitatively describes the concentrated degree of points around the linear regression line on a scatter plot. It is calculated in the following way:

$$Scatter = STD\left(2 \times \frac{X - Y}{X + Y}\right), \quad \text{(Schneider and Hase, 2011)} \quad \text{(Equation-3)}$$

and it will be used in the evaluation of the performance of SPARE-ICE in the result chapter with respect to different cloud type samples.

Apart from the typical linear regression as a comparison method, there is another approach for scientific validation: comparing the Probability Density Function (PDF) (Lary and Lait, 2006). PDFs display the distribution of the data. The bias of the compared data and their standard deviation can be qualitatively seen in the same PDF plot from the position, width and height of the curves.

To compare the differences between two groups of instantaneous or averaged data, I also calculate their Bias. It is defined as follows:

$$Bias = \frac{\sum_{i=1}^{N} (A_i - B_i)}{N}. \quad \text{(Equation-4)}$$

For the SPARE-ICE and 2C-ICE comparison in the following context, $A_i$ represents SPARE-ICE, $B_i$ represents 2C-ICE, and N is the number of samples.

For the averaged field comparison, I plot the maps of the Bias and the MFE between SPARE-ICE and 2C-IC based on their monthly mean data. With respect to the averaged field comparison between SPARE-ICE and ECHAM, more comparative methods will be introduced in the next section.

For comparisons of multiple datasets, I used a very efficient diagnostic tool: Taylor diagram, which graphically reveals how close a test dataset matches the

reference dataset. It is very useful to evaluate the performance(s) of one or multiple test datasets. The correlation coefficient, centered root-mean-square difference (RMSD) and the amplitude of the variance of data can be simultaneously represented in the Taylor Diagram.

## 4.4 Observation v.s. Model

### 4.4.1 Nash-Sutcliffe Efficiency

Nash-Sutcliffe efficiency (Nash and Sutcliffe, 1970) is a normalized statistics that compares the residual variance between the observation and model to the variance of the observation. It is a typical index extensively applied in observation and model comparison (e.g. Chen et al., 2004), and in-situ measurement and satellite measurement comparison (e.g. Krakauer et al., 2013). In model evaluation, it is expressed as

$$E = 1 - \frac{\sum_T (P_{obs}(t) - P_{\mathrm{mod}}(t))^2}{\sum_T (P_{obs}(t) - \overline{P_{obs}})^2} \qquad \text{(Equation-5)}$$

$P_{obs}$ denotes observational data, $P_{mod}$ denotes model data, and $\overline{P_{obs}}$ denotes the average of observational data.

To gain insight of the application prospect of SPARE-ICE, I use it to evaluate the IWP gained from ECHAM. When SPARE-ICE, as an observational dataset, is assumed to be the relatively accurate dataset compared to model, the performance of ECHAM can be evaluated by this Nash-Sutcliffe efficiency. If $E < 0$, it means that the model is less accurate than the observational mean; if $E=0$, it means that observation and model match and are equally precise; whereas if E is closer to 1, it means that the model has high accuracy.

### 4.4.2 Empirical Orthogonal Function (EOF) Analysis

Empirical Orthogonal Function (EOF) analysis (Lorenz, 1956) can identify patterns in data of high dimension. These patterns contribute to the large variance from the data. It decomposes a space-time field into spatial patterns and the associated

time index. Data can be split into many dimensions indicating different degrees of freedom. EOF has frequently been applied to the comparison between observation and model (e.g., Frankignoul et al., 1989; Huang et al., 2002).

As another method of SPARE-ICE and ECHAM comparison, I use the EOF analysis to display their spatial and temporal patterns, which highlight their similarities and differences. From the visualizations of different modes, we can see how many prevailing degrees of freedom of them resemble with each other; or for the same pattern, we can see if they show the same significance on their contribution to the variance of the data. The domain I chose for EOF analysis is from 66$^{o}$ south to 66$^{o}$ north, because SPARE-ICE data at latitudes beyond this domain are generally filled with 'NaN' in either pole (the reason is stated in Section 2.2).

In this study, I utilize the simple EOF analysis. The calculating procedure starts with constructing input data matrix. I subtract the annual mean from the monthly mean of the original IWP data as the input data. The temporal sampling of SPARE-ICE is different from ECHAM (SPARE-ICE one-day temporal-inconsistent granules data are not corresponding to the daily data of ECHAM). So we compare their monthly mean data. However, in the two years of overlap temporal range, the number of monthly mean data is limited. Therefore, for detrending, I simply subtract the three-point-running-mean of data, and the annual trend is not removed. In the following step, the covariance matrix and its eigenvalues and eigenvector are calculated. The Singular Value Decomposition technique is used to decompose the covariance matrix.

For the comparison, I calculate the correlation coefficient between the time index of SPARE-ICE and ECHAM. One can gain an insight of how much they are correlated with each other from both the EOF spatial pattern and temporal pattern.

EOF Analysis is a subset of the more general class of Principal Component (PC) Analysis. In my context, 'EOF' denotes the decomposed spatial pattern, and 'PC' denotes the associated time index, as often done in literatures.

# 5 Results and Discussions

## 5.1 Multi-datasets Scene Comparison

For a first qualitative evaluation, this section selects one scene in the region near to Greenland, and the case of a strong developed cyclone system with high IWP values. Figure 8 displays the scene comparisons of SPARE-ICE with MODIS, CMSAF, 2C-ICE and MSPPS IWP values parallelly. SPARE-ICE is compared with the ANN target dataset 2C-ICE, to see how well the ANN works. It is also compared to MODIS and CMSAF IWP data, which are not involved in the training of ANN. Overall, the scene maps reveal similar ice cloud texture but with different IWP magnitudes.

MODIS and CMSAF images demonstrate similar IWP magnitudes, because MODIS IWP (derived from MODIS), and CMSAF IWP (derived from AVHRR), these two products are both from the same IR+VIS technique. The small IWP values (smaller than 500 $g/m^2$, denoted by yellow) are dominant in both images. The subtle structure of the cirrus can be identified clearly.

SPARE-ICE IWP values in different orders of magnitude distribute more evenly, which shows the similar sizes of area in color (yellow denotes the small values below 500 $g/m^2$, blue denotes the medium values around 1500 $g/m^2$, and red denotes the high values around 2500 $g/m^2$), while the IWP values depicted in the 2C-ICE image are apparently higher than the values in the MODIS and SPARE-ICE images. In this cyclone case, high IWP values in all three images concentrate on the inner edge of the cyclone, where the cloud is the thickest.

The available passive microwave dataset MSPPS shows result, which is not rational, with uniformly much lower IWP values and enormous amount of missing values, which are in accordance with Eliasson et al. (2013). However, passive microwave sensors should be capable to detect the large particles in the lower part of the cloud. That is to say, the quality of this product remains controversial. Therefore, the following results exclude the comparison between SPARE-ICE and passive microwave IWP products.

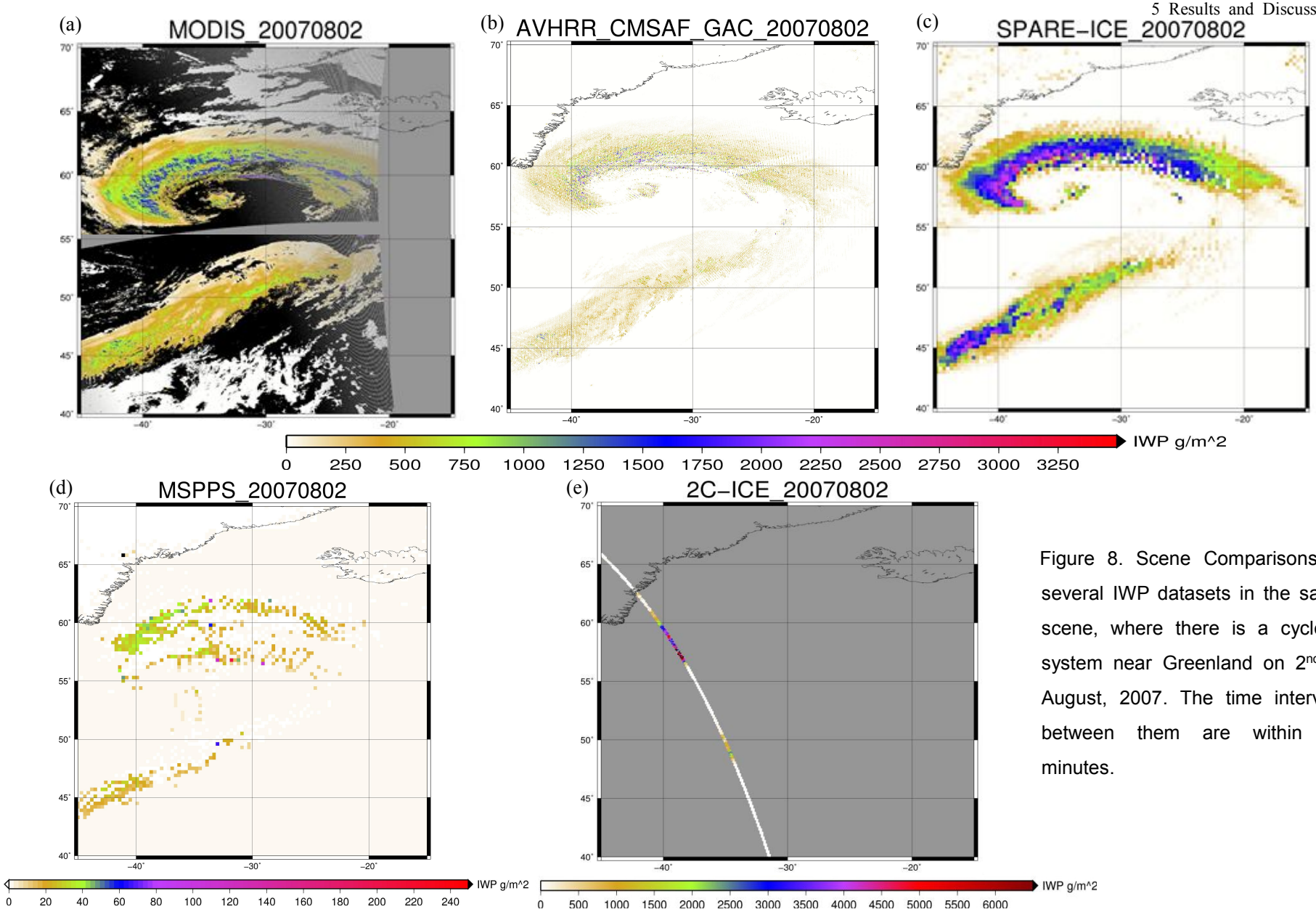


Figure 8. Scene Comparisons of several IWP datasets in the same scene, where there is a cyclone system near Greenland on 2nd of August, 2007. The time intervals between them are within 15 minutes.

## 5.2 SPARE-ICE v.s. 2C-ICE

Since the case in the scene comparison is chosen at high latitudes, it is only partly representative, to have a rigorous and comprehensive comparison and more convincible results, the comparisons should be in a larger spatial and temporal scale. In this section, I do the comparison with the collocated samples in a whole year of 2008, in different regions on the global scale and in the low latitude region between $30^o$ north and $30^o$ south, to see the difference of SPARE-ICE in latitudes.

Figure 9 is the 2D-histogram of SPARE-ICE and 2C-ICE comparison based on the global samples (Figure 9 (a)) and tropical samples (Figure 9 (b)). Even though SPARE-ICE data do not fit 2C-ICE data completely, the Linear Regression shows high correlations. The correlation coefficients between SPARE-ICE and 2C-ICE in Figure 9 (a) and (b) are 0.79 and 0.89, respectively, both approaching value one, and their medians of fractional error are very low, around 0.11 and 0.08, respectively. At low latitudes, the correlation coefficient is higher, and the median of fractional error is smaller than for the globe. The areas denoted by both, blue and red color, shrinking from (a) to (b), also tell us the same truth that the samples at low latitudes are more concentrated. The median curves of SPARE-ICE and 2C-ICE as well as the linear regression line in Figure 9 (b) almost coincide with each other from 100 $g/m^2$ onward, while in Figure 9 (a), the three lines slightly depart from each other, and both median curves of SPARE-ICE and 2C-ICE bend to the axis of 2C-ICE, indicating 2C-ICE IWP values are larger than SPARE-ICE IWP based on all samples. This is a result from the much higher IWP values of 2C-ICE than SPARE-ICE at high latitudes. It agrees with the result of the scene comparison in Section 5.1. However the small IWP values are still not represented very well in SPARE-ICE. SPARE-ICE data are larger than 2C-ICE for small values. The reason still remains to be discussed. As speculation, one possible reason is that AVHRR sounding channels regard the Earth surface snow cover as cloud ice. Overall, the result from Figure 9, based on the data of 2008 shows very high correlation between SPARE-ICE and 2C-ICE as expected, and this is in conformity to the result of Holl et al. (2014), which used the data of 2007.

(a)

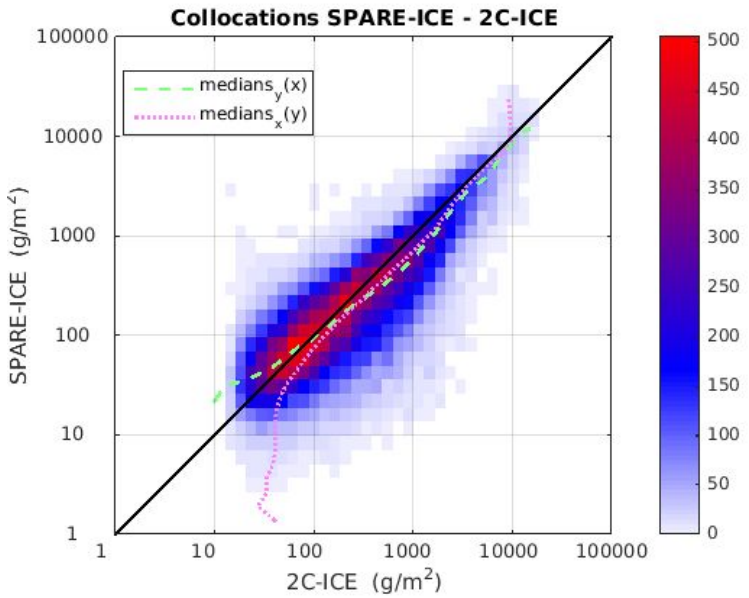


ρ=0.79 MFE=0.11

(b)

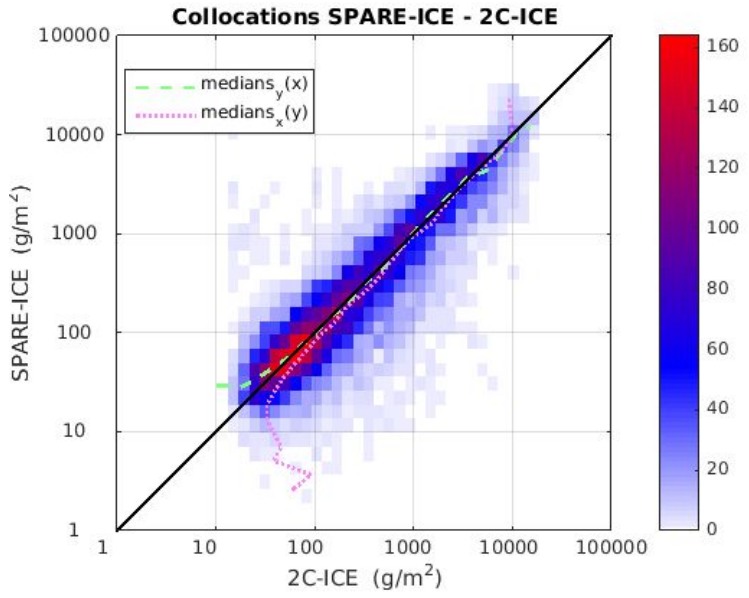


ρ=0.89, MFE=0.08

Figure 9. 2D-Histogram of the comparisons between 2C-ICE and SPARE-ICE based on the collocations in 2008. (a): globe; (b): low latitudes between -30° and 30°. The green dash line represents the median of SPARE-ICE; the pink dash line represents the median of 2C-ICE.

By plotting the PDFs of SPARE-ICE and 2C-ICE with respect to the samples at different latitudes, as shown in Figure 10, it is more convenient to compare the distributions of the IWP values. Both SPARE-ICE and 2C-ICE data tend to be a log-normal distribution. Comparing to SPARE-ICE, the magnitudes of 2C-ICE data are relatively more widely spread, and showing lower frequency at the center. The missing small values (below 1 $g/m^2$) of SPARE-ICE can be seen. At mid- and high latitudes, the SPARE-ICE and 2C-ICE IWP values are more concentrated near 100 $g/m^2$, and there is a shift of the curves of SPARE-ICE and 2C-ICE between the 1000 and 10000 $g/m^2$. Although this shift is not large in log-normal scale, but indicates the value of IWP of 2C-ICE has much larger observational frequency than SPARE-ICE in this range of value at mid- and high latitudes. The SPARE-ICE and 2C-ICE IWP values are more concentrated between 10 to 100 $g/m^2$ at low latitudes. SPARE-ICE data have almost the same probability density as 2C-ICE at low latitudes between the IWP value of 1000 to 10000, as shown by the second submit of the SPARE-ICE curve in Figure 10 (c). Overall, from the PDFs, we cannot see very apparent bias between SPARE-ICE and 2C-ICE.

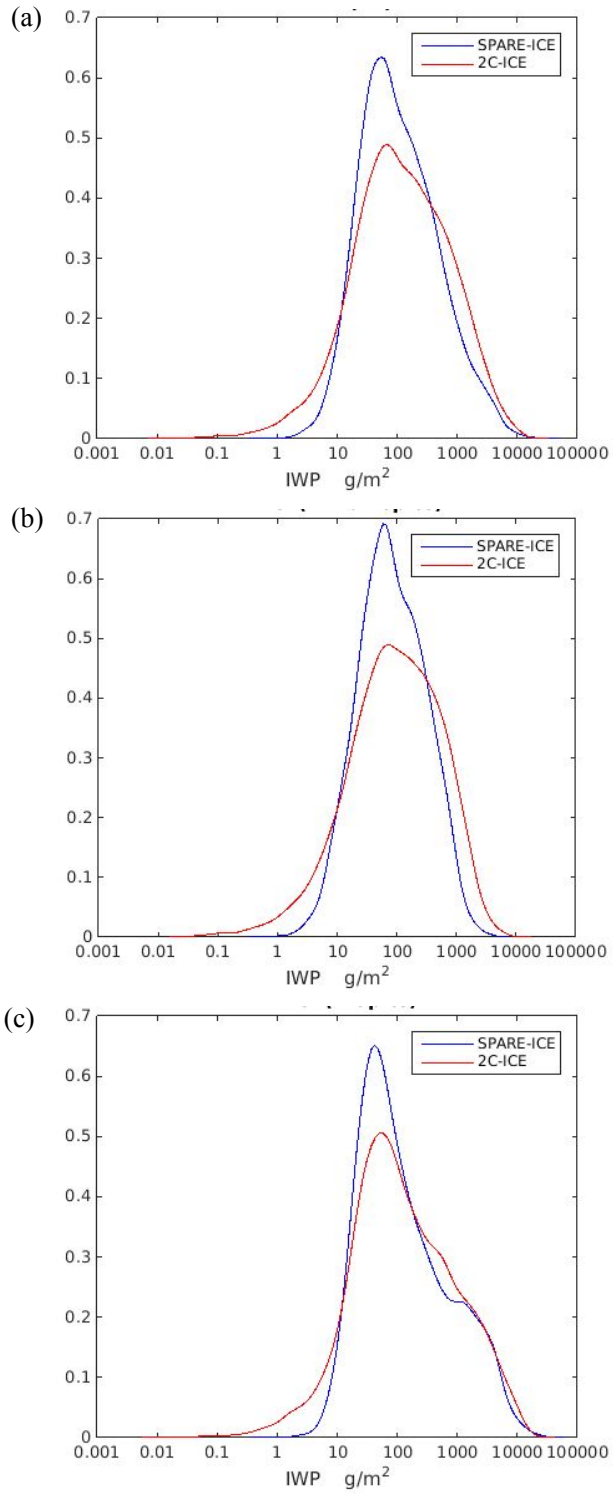


Figure 10. PDFs of collocated SPARE-ICE and 2C-ICE samples in (a) globe, (b) mid- and high latitudes and (c) low latitudes, 2008.

From the results above, we notice that the high correlation and small MFE are shown at low latitudes, where the majority of convective clouds with high uncertainty in IWP retrieval are located. In other words, the performance of SPARE-ICE seems

not vulnerable to the uncertainty in convective cloud ice retrieval. To see the performance of SPARE-ICE in terms of different cloud types and to analyze the outliers in Figure 9 in depth, this section also shows the SPARE-ICE and 2C-ICE comparisons concerning different cloud types and time intervals, as shown in Figure 11 and Table 4. The low latitude region is chosen for this comparison due to the better performance of SPARE-ICE compared to the globe.

Figure 11 presents the cloud samples, which meet the following criteria: Horizontally, only one type of cloud within one large footprint; vertically, only one type of cloud in the cloud column (no mixing with other type of clouds in different layers). I use these criteria rather than setting a specific threshold for the standard deviation (STD) of the IWP values within one large footprint, because the magnitudes of STD is highly dependent on cloud types. For instance, the relatively homogeneous convective cloud has larger STD than the relatively inhomogeneous cirrus.

The smaller the time interval, the more stringent is the collocation. Therefore, as expected, after narrowing down the time interval from 600 s to 120 s, the correlation coefficient of the samples from deep convection, cirrus and altostratus increase to 0.8046 from 0.6634, 0.8260 from 0.1174, and 0.8656 from 0.8420, respectively, and all higher and larger than 0.8, as shown in Table 4. For these three cloud types, including the deep convection samples, which have largest uncertainty in cloud ice retrieval, narrowing down the time threshold can diminish most of the wide spread points (the number of points are reduced from 580 to 117, from 2061 to 385, and from 920 to 170), for deep convection, cirrus and altostratus, respectively). It also contributes to smaller bias for deep convection (from 376.88 $g/m^2$ to -74.71 $g/m^2$) but larger bias for cirrus (from -12.47 $g/m^2$ to 19.68 $g/m^2$) and altostratus (from 22.85 $g/m^2$ to 38.79 $g/m^2$). The scatters of these three cloud types also decrease after narrowing down the time threshold, from 0.5029 to 0.4957 for deep convection, from 0.7729 to 0.5223 for cirrus, and from 0.5800 to 0.5120 for altostratus. It turns out that the correlation coefficient and scatter between SPARE-ICE and 2C-ICE have no large difference for different cloud types.

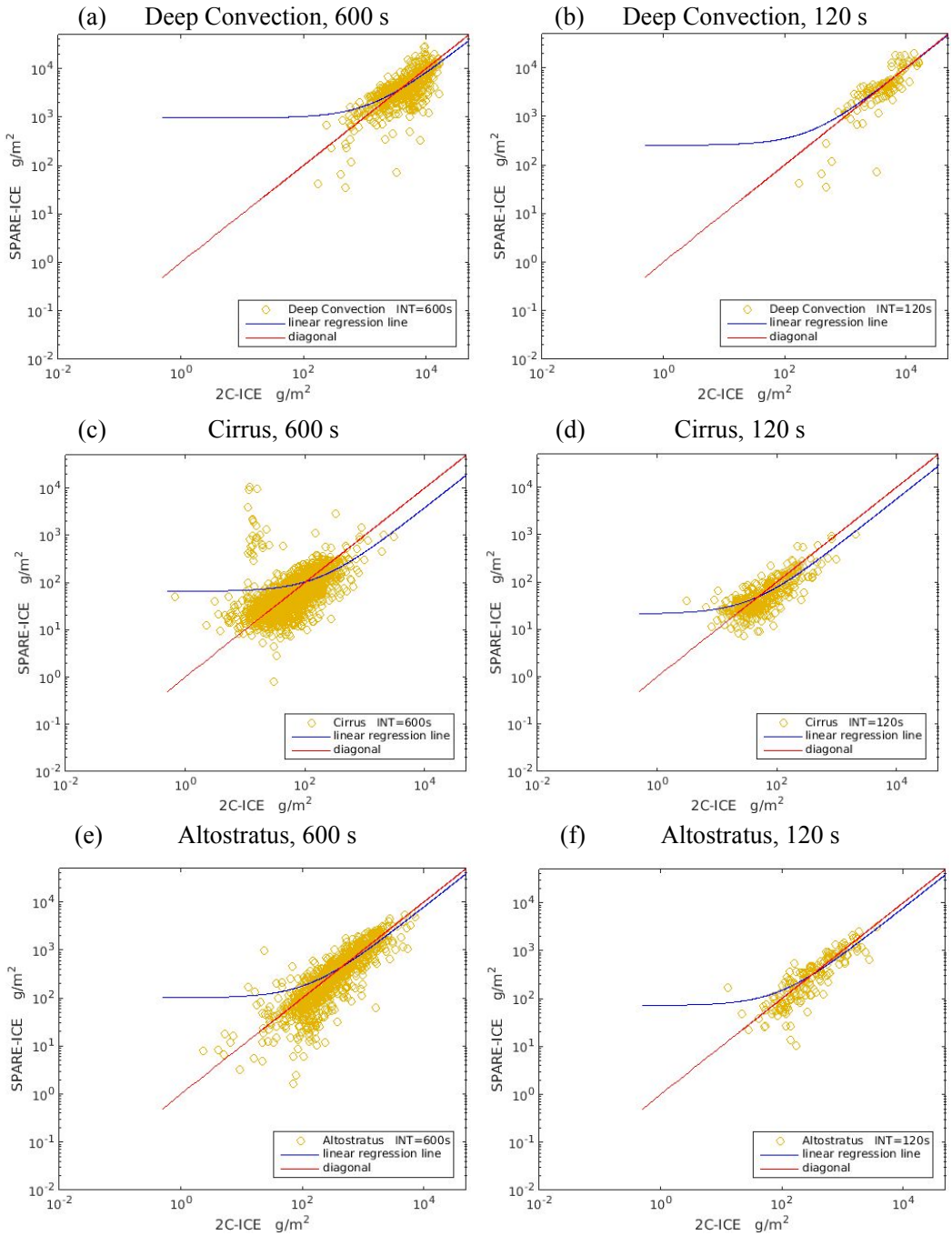


Figure 11. Scatter plots of SPARE-ICE and 2C-ICE comparison in different cloud categories and the temporal thresholds of collocation within 600 s and 120 s.

Table 4. Comparisons between SPARE-ICE and 2C-ICE for different cloud types and temporal thresholds of collocation

| | Deep Convection | | Cirrus | | Altostratus | |
|---|---|---|---|---|---|---|
| Time interval | 600 s | 120 s | 600 s | 120 s | 600 s | 120 s |
| No. of Samples | 580 | 117 | 2061 | 385 | 920 | 170 |
| Correlation Coef. | 0.6634 | 0.8046 | 0.1174 | 0.8260 | 0.8420 | 0.8656 |
| Bias* | 376.8786 | -74.7104 | -12.4681 | 19.6827 | 22.8538 | 38.7898 |
| Scatter | 0.5029 | 0.4957 | 0.7729 | 0.5223 | 0.5800 | 0.5120 |

* Bias: mean of the difference between 2C-ICE and SPARE-ICE

Further averaged field comparisons between SPARE-ICE and 2C-ICE are shown in Figure 12 and Figure 13. Figure 12 presents the global distribution of annual gridded mean SPARE-ICE and 2C-ICE data. From the map of SPARE-ICE, we can observe apparent double ITCZ, which is also shown on the map of 2C-ICE. High values in Amazon Basin also highlight both maps. However the texture of ice clouds on gridded map of 2C-ICE is not as smooth as on gridded map of SPARE-ICE, due to the poor sampling effect of CloudSat and CALIPSO. After calculating the average by ignoring NaN values, 2C-ICE data are spatially discontinuous, so that in the annual mean map, many high IWP value textures cannot be smoothed.

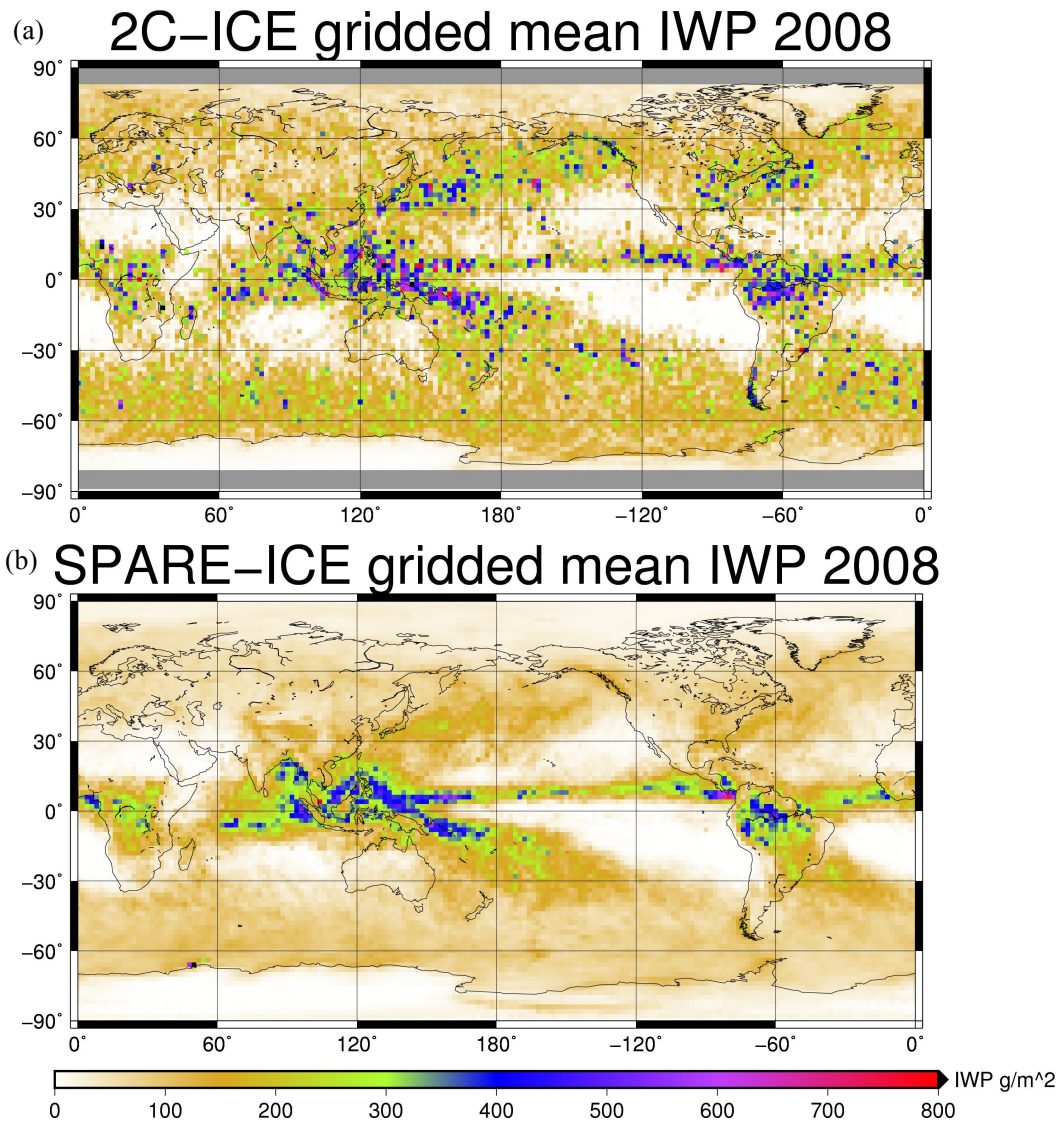


Figure 12. Maps of (a) SPARE-ICE and (b) 2C-ICE IWP based on 2008 annually gridded mean data.

Figure 13 (a) portrays the medians of fractional error calculated from the gridded monthly mean SPARE-ICE and 2C-ICE data. If both SPARE-ICE and 2C-ICE IWP values are small, although their absolute difference is small, their FE might be very large. The white color regions therefore denote the regions where ice clouds rarely exist. For the ice cloud prevailing regions, their medians of fractional error range from 0 to 3, corresponding to 1:1 to 4:1 magnitude ratio, and present a random spatial distribution.

However, the map of Bias between SPARE-ICE and 2C-ICE, as shown in Figure 13 (b), observes that positive biases are predominant in tropics (The IWP bias of many grid-points in the double ITCZ region reaches 200 g/m$^2$), while negative biases

are predominant at mid- and high latitudes. These IWP bias reach -200 g/m$^2$ in North Pacific and east of the North America. From Figure 14, we can see the zonal mean of 2C-ICE and SPARE-ICE agree well with each other in low latitudes (between 20$^o$ south to 20$^o$ north) but has large disagreement between 20$^o$ north and 80$^o$ north, and between 20$^o$ south and 70$^o$ south. In these two extra-tropics regions, 2C-ICE data have the higher zonal mean (maximum of around 150 g/m$^2$) than SPARE-ICE, and SPARE-ICE data have the lower zonal mean, around 100 g/m$^2$, than 2C-ICE. The zonal mean curve of ECHAM will be analyzed in Section 5.4. From both figures, we can confirm that, the performance of SPARE-ICE is better at low than at high latitudes.

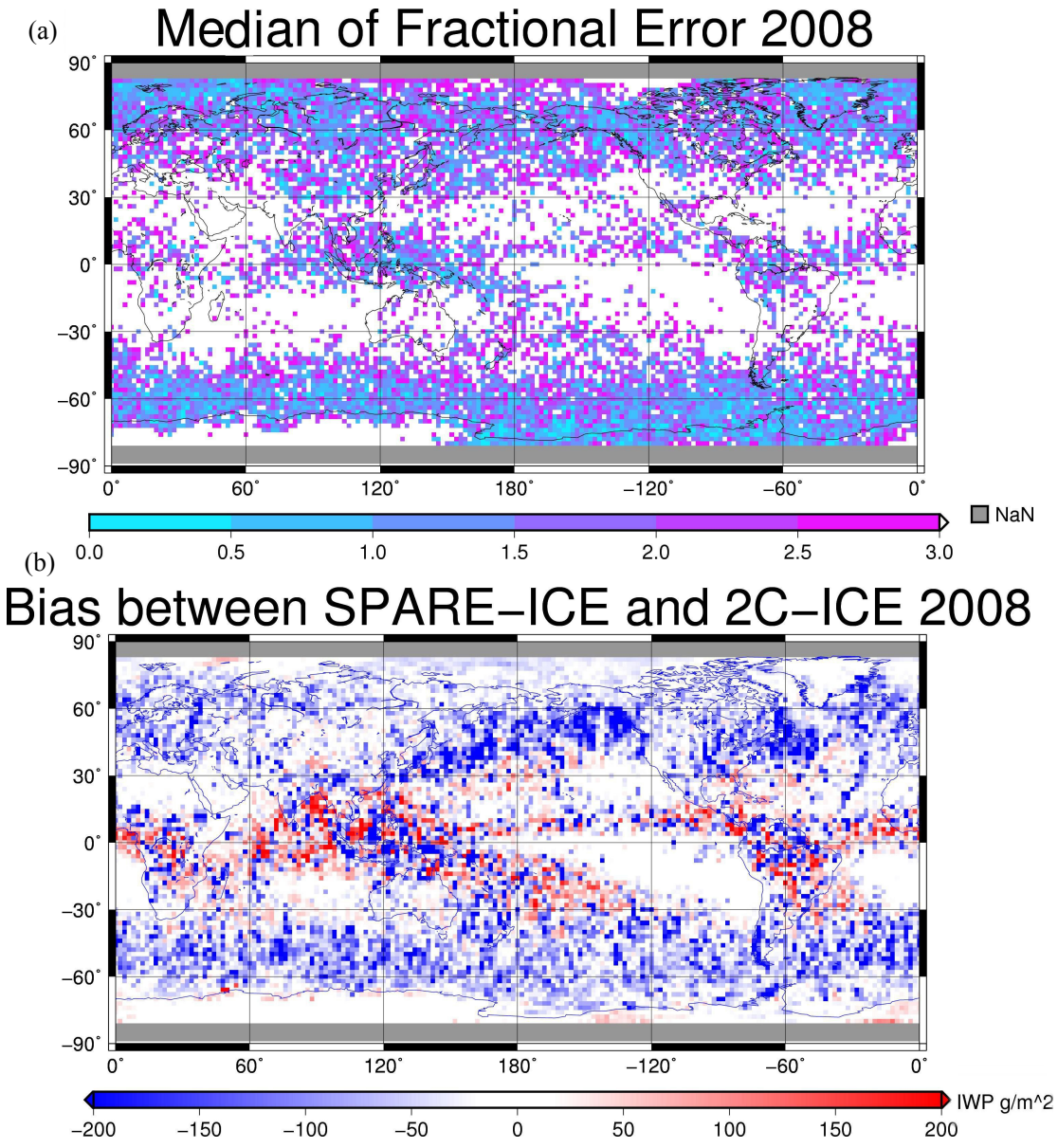


Figure 13. Maps of (a) MFE and (b) Bias between SPARE-ICE and 2C-ICE calculated from 2008 gridded monthly mean data.

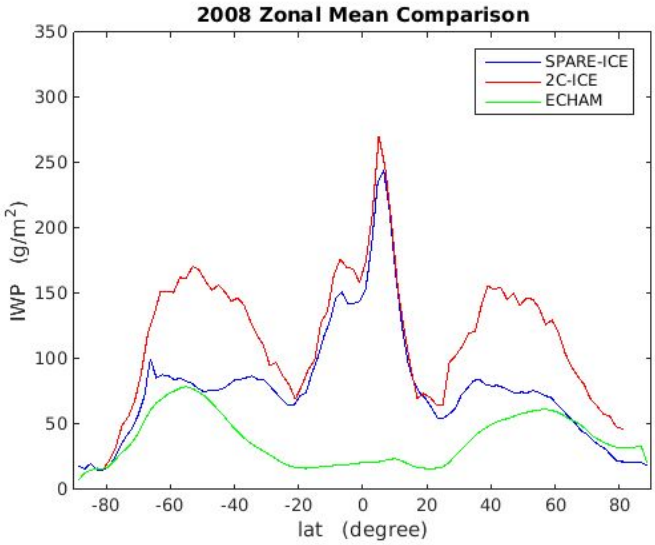


Figure 14. Zonal mean comparison between SPARE-ICE, 2C-ICE and ECHAM.

I can only speculate on the reasons accounting for this phenomenon: Firstly, the concentration of water vapors is higher at low latitudes than at high latitudes. The ice cloud detection for the microwave channels is in favor of humidity in the atmosphere. When the atmosphere is dry, the sounding channels of microwave sensors can sense the Earth surface and hence the difference of radiance between the sounding channel and the surface sensitive channel is smaller than in the humid atmosphere condition. Therefore, the IWP values in such regions tend to be underestimated. Secondly, the Earth surface temperature is higher at low latitudes than at high latitudes. The infrared channels are more sensitive to ice clouds when the surface is warm, because they rely on a thermal contrast between cloud tops and Earth surface, and this contrast is much larger at low latitudes than at high latitudes, especially in winter. Additionally, the IWP values are higher at low latitudes than at high latitudes. SPARE-ICE performs better for large values of IWP, because the microwave channels are only sensitive to large ice particles.

## 5.3 SPARE-ICE v.s. MODIS

Figure 15 shows the collocated one day samples between SPARE-ICE and MODIS data on January 11$^{th}$ of 2008. It is the collocated version of scene comparison,

and has larger scene (covering tropics, extra-tropics and Antarctic) and smaller time interval than in Section 5.1. SPARE-ICE IWP values are apparently higher than MODIS in tropics, because MODIS is not capable of detecting the whole range of the strong convective clouds. The MODIS image shows many ice clouds over Antarctic. However, the SPARE-ICE image doesn't show those anomalous IWP values. As speculation, one possible reason for this phenomenon is that the algorithm of MODIS IWP retrieval regards the ice sheet or snow cover as cloud ice under the circumstance of dry air condition (Eliasson et al., 2011).

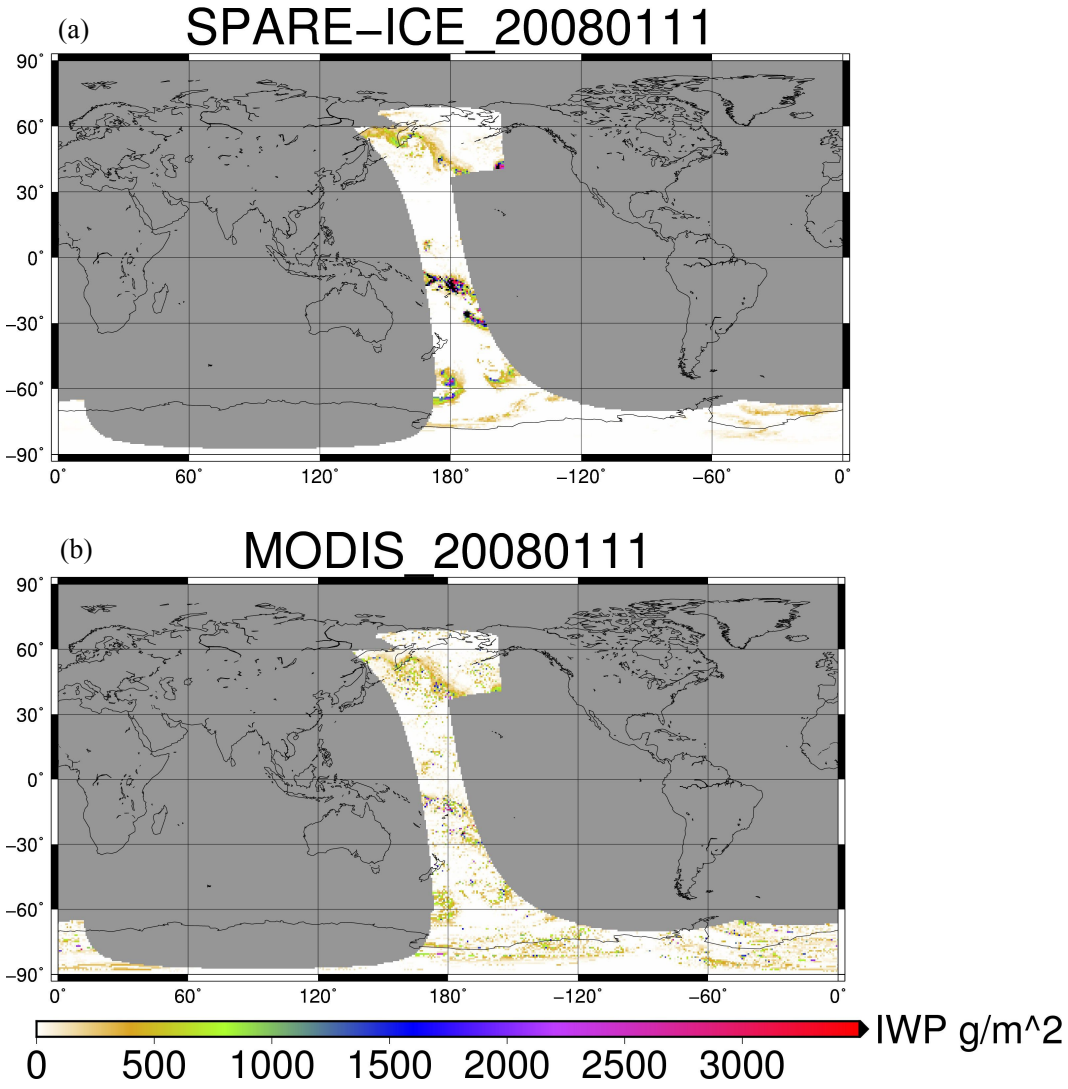


Figure 15. Maps of collocated (a) SPARE-ICE and (b) MODIS data on Jan. 11th, 2008.

From Figure 16, we can see that, although the correlation coefficient of MODIS and SPARE-ICE comparison is 0.5150, which is relatively small, it shows an apparent linear trend with a slope larger than 1. The general trend deviates off the diagonal from around 100 g/m$^2$. The median of fractional error is 0.1939, which is smaller than 0.2 and satisfying. A small fraction of points is widely scattered, showing the scatter

density denoted by light blue color. In general, SPARE-ICE data tend to be larger than MODIS data for the large IWP values (larger than around 100 g/m$^2$ for MODIS). It benefits from the 2C-ICE dataset as retrieval reference. For the small IWP values, MODIS data are higher than SPARE-ICE IWP. One speculative reason could be the footprint size difference between MHS (or AVHRR) and MODIS. Both MHS and AVHRR are detecting the brightness temperature to retrieve IWP. Their larger footprints compared to MODIS allow them to receive the brightness temperature from the Earth surface. That is to say, the overall signal received from each footprint indicates the averaged brightness temperature of clouds and the Earth surface. Hence, for clouds in a horizontal scale smaller than the footprint of MHS, SPARE-ICE IWP is probably underestimated.

Figure 17 is the PDF of the collocated SPARE-ICE and MODIS. The two curves have higher similarity in their probability density than the ones from SPARE-ICE and MODIS shown in Figure 10 and approximately similar. A lower peak happens on the blue curve denoting SPARE-ICE between 1000 to 10000 g/m$^2$, indicating SPARE-ICE has more values than MODIS within this range of magnitude. This phenomenon could be attributed to thick clouds. Again, the PDF also shows that SPARE-ICE is lack of small values below 1 g/m$^2$.

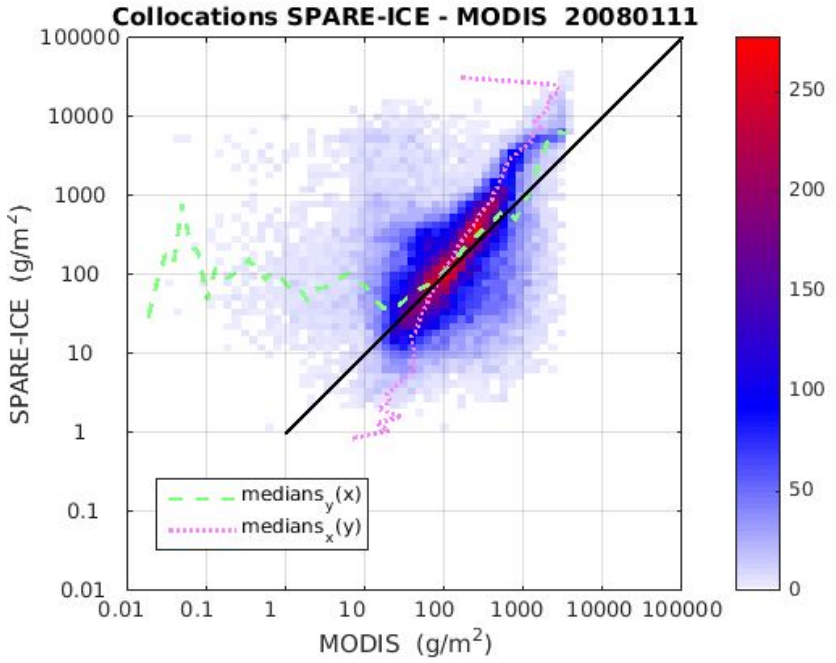


ρ=0.5150; MFE=0.1939

Figure 16. 2D-Histogram of the comparison between SPARE-ICE and MODIS based on the collocations on Jan. 11th, 2008. The green dash line represents the median of SPARE-ICE; the pink dash line represents the median of 2C-ICE.

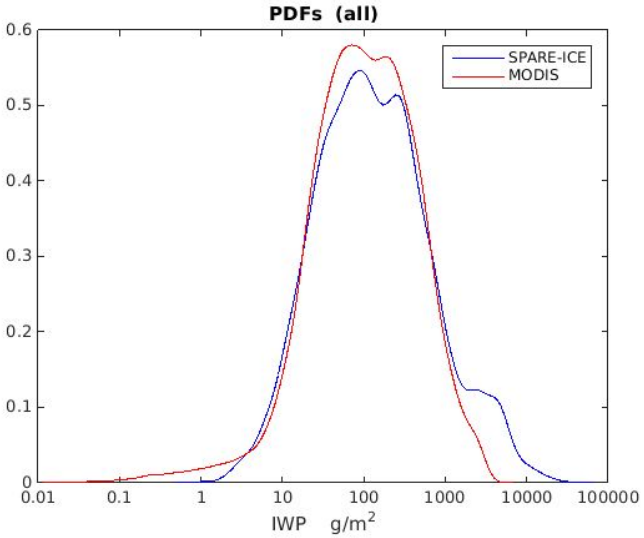


Figure 17. PDFs of collocated SPARE-ICE and MODIS samples on Jan. 11st, 2008.

In order to achieve a relatively parallel evaluation of SPARE-ICE with 2C-ICE, and with MODIS, this section presents the Taylor Diagram for both comparisons as shown in Figure 18. Note that the collocated SPARE-ICE samples used for comparisons with 2C-ICE and MODIS in Figure 18 are not based on a consistent temporal range (one year data of 2008 and one day data of Jan. 11$^{th}$, 2008, respectively). The Taylor Diagrams demonstrate that the standard deviation of SPARE-ICE (about 1600 g/m$^2$) is clearly greater than the standard deviation of MODIS (about 400 g/m$^2$). 2C-ICE (with STD of 1600 g/m$^2$) has almost identical standard deviation as SPARE-ICE. It indicates that the variability of SPARE-ICE data assembles the variability of 2C-ICE data, but both of them are far away larger than the variability of MODIS data. The RMSD between SPARE-ICE and 2C-ICE is about 900 g/m$^2$, which is much smaller than the RMSD between SPARE-ICE and ECHAM, about 1400 g/m$^2$. Moreover, the correlation coefficient between SPARE-ICE and 2C-ICE is about 0.83, which is much larger than the correlation coefficient between SPARE-ICE and MODIS, about 0.52. The distance (determined by both the RMSD and the correlation) between SPARE-ICE and 2C-ICE is shorter than the distance between SPARE-ICE and MODIS. It reveals that SPARE-ICE and 2C-ICE have much more agreement than SPARE-ICE and MODIS.

The comparisons have shown SPARE-ICE is a reliable dataset. Therefore, it can be used for evaluation of model in the next section.

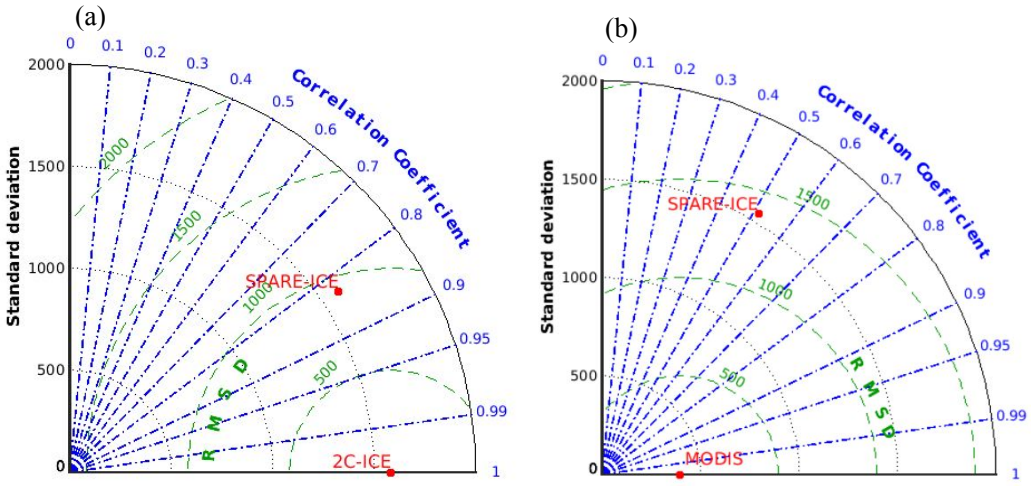


Figure 18. Taylor diagram of SPARE-ICE compared with (a) 2C-ICE and with (b) MODIS. Unit for RMSD and STD: g/m$^2$

## 5.4 Application: Evaluating ECHAM with SPARE-ICE

Figure 19 is the map of annually averaged ECHAM IWP. It exhibits several high value regions: Tibet Plateau, Rocky Mountain, Patagonia in South America, as well as the westerlies regions in northern and southern hemisphere. Differing from the gridded maps of SPARE-ICE and 2C-ICE, in the map of ECHAM, the entire ITCZ appears to be missing. Particularly, the magnitude of IWP as shown in Figure 19 is uniformly and substantially smaller than the magnitude of SPARE-ICE IWP as shown in Figure 12 (b). The zonal means of ECHAM, as shown in Figure 14, between 20$^o$ north and 20$^o$ south, are around 20 g/m$^2$, which are substantially smaller than 2C-ICE and SPARE-ICE. With the increase of latitudes till 60$^o$, they approach the value of 2C-ICE and SPARE-ICE, and reach the maximum of about 80 g/m$^2$, but still smaller than them. When the latitude goes beyond 60$^o$, the zonal mean values of these three datasets become relatively close. The zonal mean curves of 2C-ICE and ECHAM are however qualitatively consistent with the results in Eliasson et al. (2010).

ECHAM data show significantly low values in tropics compared to SPARE-ICE. There are several possible reasons. The primary reason is that ECHAM excludes precipitating ice particles such as snow from ice cloud when calculating IWP. Secondarily, the cloud fraction is smaller (Eliasson et al., 2010), due to the relatively small horizontal scale of convective clouds. Moreover, ECHAM cannot resolve very

small scale of variability. As stated by Stevens et al. (2002), “major biases appear to be limited by the parameterization of small-scale physical processes, such as clouds and convection”. However, many convective cells in tropics are very small compared to the horizontal grid cell of ECHAM (about 208 km × 208 km at the equator).

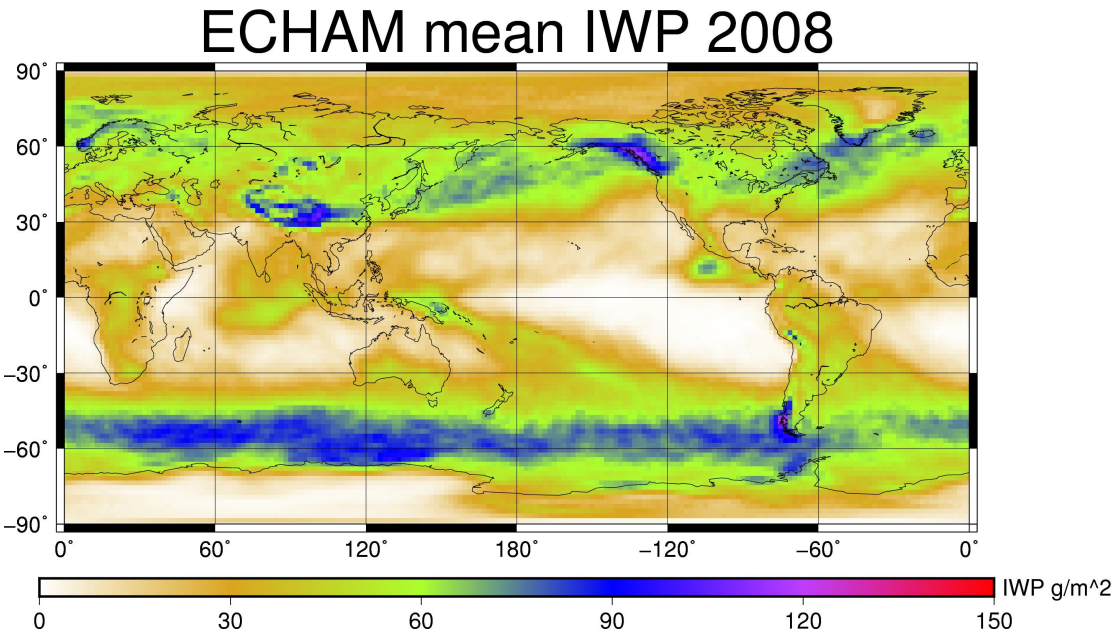


Figure 19. Map of ECHAM annually mean IWP data in 2008.

The Nash-Sutcliffe efficiency as shown in Figure 20 evaluates the model when the observation is assumed to be accurate. The positive Nash-Sutcliffe efficiency (between value 0 to 1) tends to be located in central Asia, South Africa, south Indian Ocean and Chile Basin of south Pacific. It implies that ECHAM and SPARE-ICE have higher agreement in these regions. In other words, if SPARE-ICE is assumed to be the accurate dataset, then ECHAM is evaluated to be also accurate in these regions. The negative Nash-Sutcliffe efficiency tends to be in the ITCZ, North Africa, Arabia, south Atlantic and Peru Basin of south Pacific. It indicates that ECHAM and SPARE-ICE have large disagreements in these regions, and therefore that ECHAM is less accurate there.

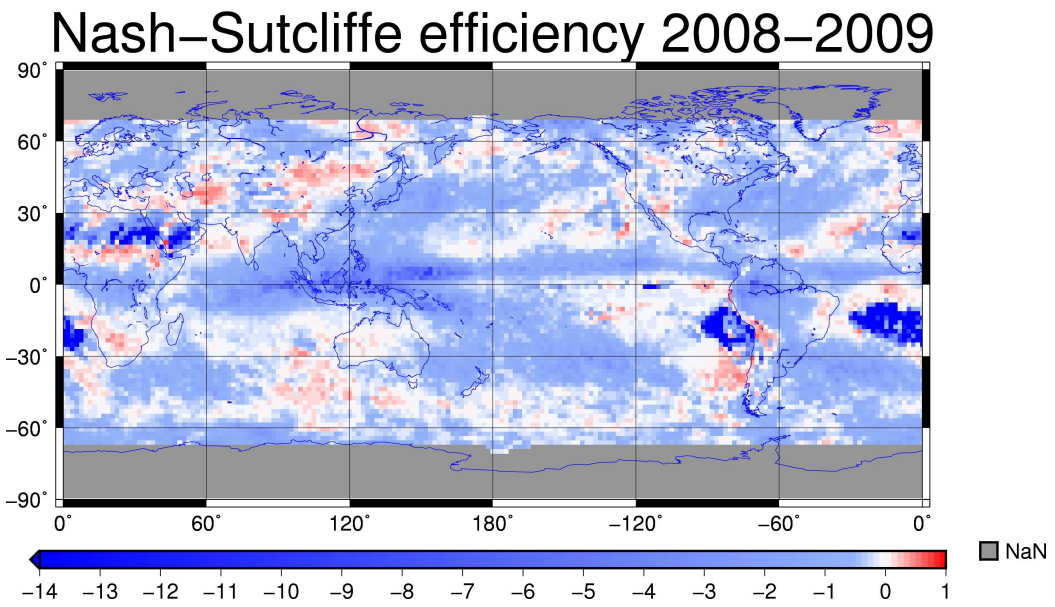


Figure 20. Map of Nash-Sutcliffe efficiency between SPARE-ICE and ECHAM monthly gridded mean data from 2008 to 2009.

Figure 21 depicts two years of annual variation of SPARE-ICE and ECHAM. For the selected domain, which is in the westerlies and oceanic region, although SPARE-ICE and ECHAM deviate from each other by about 80 g/m$^2$ in winter and about 60 g/m$^2$ in summer, their monthly variations follow the same trend. Both display a clear annual cycle, with the maxima in winter and minima in summer.

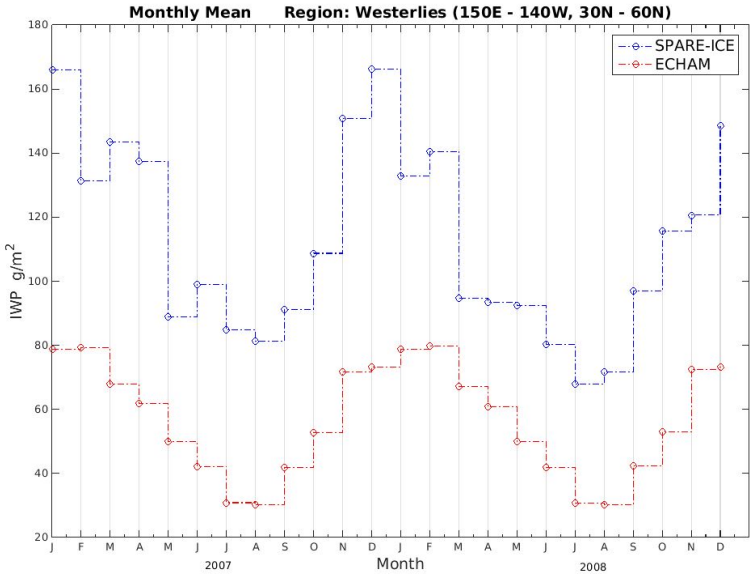


Figure 21. Annual variation of IWP in Northern Hemisphere Westerlies region, based on muti-years monthly mean data from January of 2007 to December of 2008. (Blue line: SPARE-ICE; red line: ECHAM).

From the seasonal variation of SPARE-ICE IWP and ECHAM IWP as shown in Figure 22 and 23, respectively, we can clearly see the monsoon cycle over Asian Bay of Bengal and Sahel, and the ITCZ seasonal displacement can be observed in the Indo-Pacific warm pool. The northern hemisphere westerlies and southern hemisphere westerlies regions are highlighted by the high IWP values in Figure 23 for four seasons, weakest in southern hemisphere summer and strongest in southern hemisphere winter.

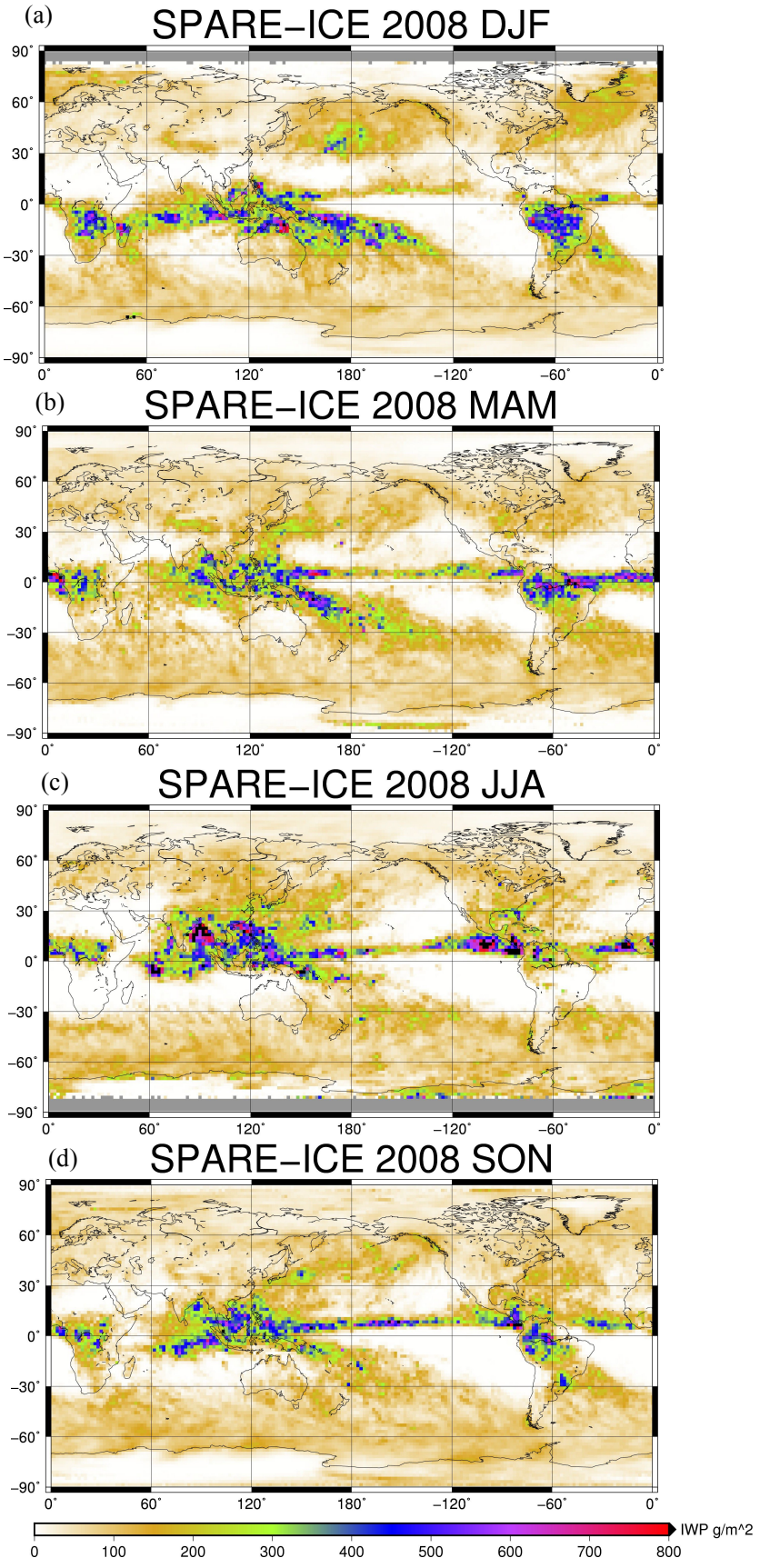


Figure 22. Seasonal variation of SPARE-ICE IWP in 2008.

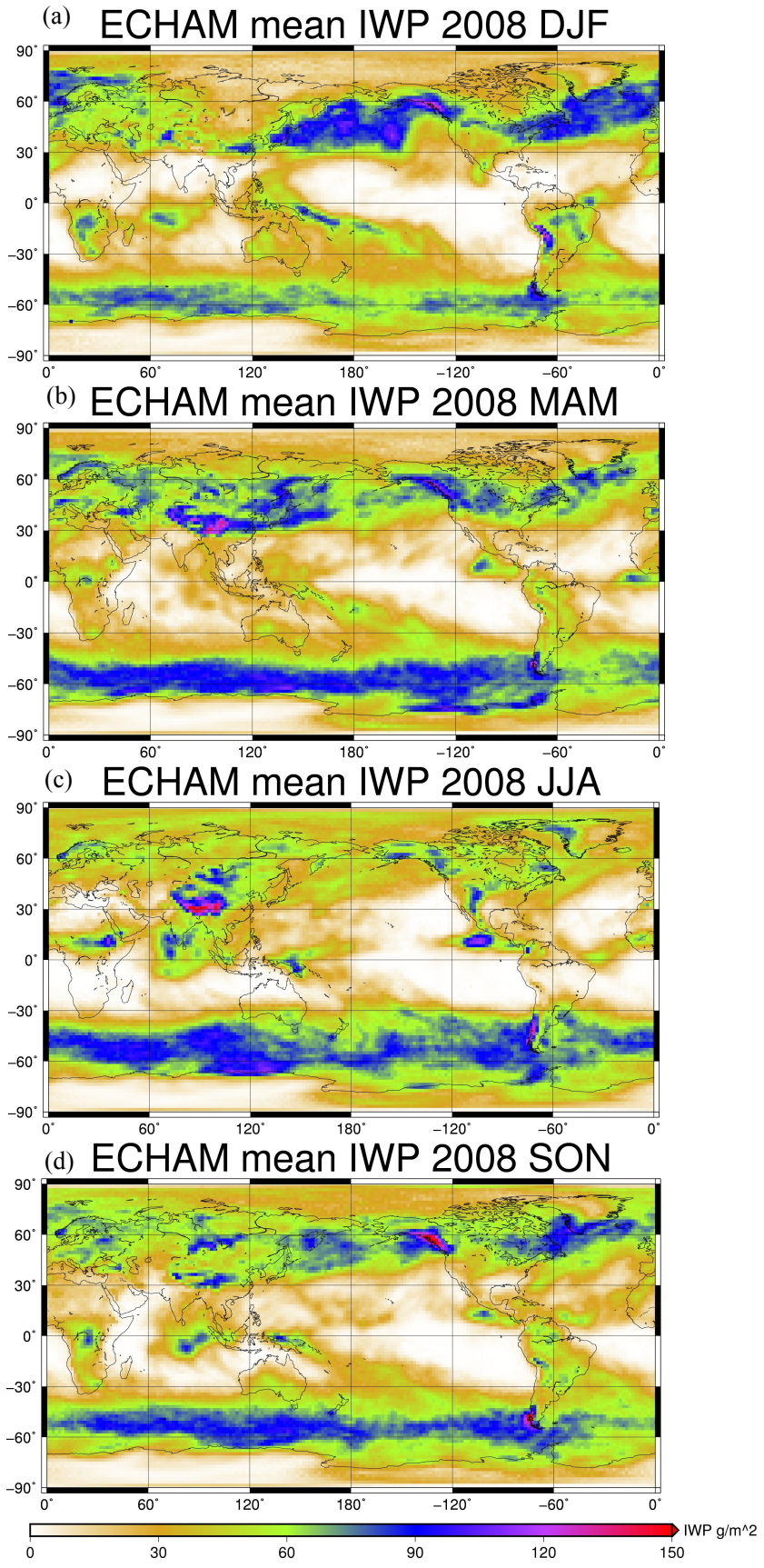


Figure 23. Seasonal variation of ECHAM IWP in 2008.

Apart from the seasonal variation observed above, another question worthwhile to investigate is if SPARE-ICE and ECHAM are both able to identify the other resemblant patterns. Therefore, I conduct the EOF analysis using two years of monthly mean SPARE-ICE and ECHAM data. The decomposed spatial patterns are shown in Figure 24. The correlation coefficients of the decomposed temporal patterns between ECHAM and SPARE-ICE are shown in Table 5, and the percentages of variance of SPARE-ICE and ECHAM in EOF analysis are shown in Table 6.

From the first EOF spatial modes, i.e. the dominant pattern in the IWP of SPARE-ICE and ECHAM depict a strong resemblance in southern hemisphere and northern hemisphere, apart from the regions around the Philippine Sea and the Tibet Plateau. For example, ECHAM data emphasize that Tibet Plateau contributes to large variability of IWP, while SPARE-ICE data do not show. The seasonal variation from the atmospheric circulation is observed, e.g. over Africa. It worthwhile to notice that the spatial pattern might imply that the ITCZ shifts north and south. Since there are only two years of overlapped SPARE-ICE and ECHAM data available, I did not subtract the annual trend. That is why the seasonal variation can be observed on the first mode. However, on the second EOF spatial mode, the resemblance is much smaller than on the first EOF spatial mode, and the physical meaning of the presented second modes of both SPARE-ICE and ECHAM are not clearly understood.

From the EOF temporal patterns, as shown in Table 5, we can see the correlation coefficients between the first, second, third and fourth EOF temporal modes of SPARE-ICE and ECHAM are 0.9220, 0.8761, -0.3002 and -0.3911, respectively. Both the first and the second EOF temporal modes of SPARE-ICE have a very high correlation with ECHAM. It implies that SPARE-ICE data resemble ECHAM data for the first two leading EOF modes in temporal patterns.

Additionally, the percentages of variance for each pair of corresponding modes, as shown in Table 6, have not much difference. It indicates that for both datasets, the corresponding modes attribute to similar extent of variance of IWP data.

Overall, due to the similar variability features resolved from both datasets by EOF analysis, we can argue that the simulated pattern of ECHAM matches well with the observational dataset SPARE-ICE. Therefore, SPARE-ICE can well be used for evaluation of model and is a very valuable dataset.

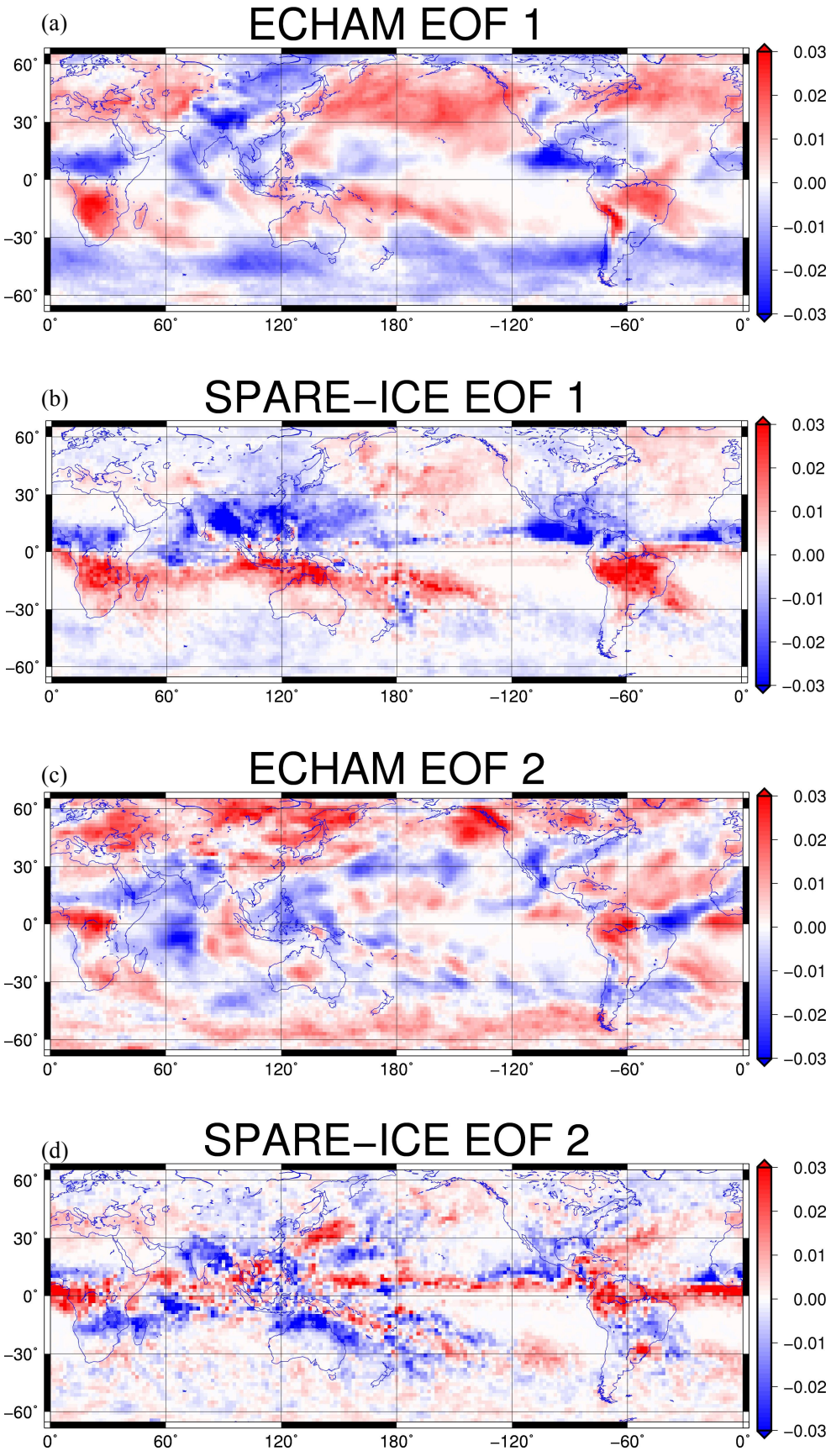


Figure 24. EOF spatial patterns of SPARE-ICE and ECHAM for the first two predominant modes

Table 5. Correlation Coefficients between the EOF temporal coefficients of SPARE-ICE and ECHAM for respective modes

| | Mode 1 | Mode 2 | Mode 3 | Mode 4 |
|---|---|---|---|---|
| Correlation Coefficient | 0.9220 | 0.8761 | -0.3002 | -0.3911 |

Table 6. Percentage of variance for SPARE-ICE and ECHAM in EOF analysis

| Eigenvalue (%) | SPARE-ICE | ECHAM |
|---|---|---|
| Mode 1 | 37.3 | 34.7 |
| Mode 2 | 24.2 | 24.3 |
| Mode 3 | 19.8 | 22.3 |
| Mode 4 | 18.5 | 18.6 |

# 6 Conclusions

In this study, with the SAPRE-ICE retrieval algorithm developed by Holl et al. (2014), I processed the SPARE-ICE data from 2006 to 2009 (excluding 2007). The performance of SPARE-ICE product is evaluated with the new processed data by comparing to the several IWP observational datasets, and its application value is demonstrated by comparing to ECHAM model.

After a scene comparison, it is obvious that the IWP values on SPARE-ICE, 2C-ICE, MSPPS, MODIS and AVHRR-CMSAF image demonstrate similar ice cloud texture but different IWP magnitudes. IWP in different order of magnitudes distribute more evenly on SPARE-ICE image, which shows not only the low value characteristics like MODIS and AVHRR, but also the high value characteristics approaching 2C-ICE.

A rigorous intercomparison of SPARE-ICE against other datasets is performed by using linear regression. The result shows that the new processed SPARE-ICE data of 2008, which are from the Neural network trained by Holl et al. (2014) based on the data of 2007, have an extremely high degree of correlation with 2C-ICE data. That is to say, the SPARE-ICE retrieval is well conducted. Moreover, for different cloud types, SPARE-ICE has consistently good performance. The principal reason for the appearance of outlier is the relatively large time threshold for collocation, and this factor has nothing to do with the performance of SPARE-ICE.

As speculation, Earth surface and cloud temperature contrast, atmospheric humidity and cloud droplet size distribution are essential factors, which account for the performance difference of SPARE-ICE at different latitudes, as seen from the comparison of SPARE-ICE and 2C-ICE.

In general, according to the nature of different techniques, the comparison result between SPARE-ICE and MODIS is reasonable, but it shows that their small IWP values differ. SPARE-ICE combining MHS and AVHRR techniques can detect the lower part of clouds benefiting from MHS, while both individual MODIS and AVHRR cannot achieve; and 2C-ICE combining RADAR and LIDAR techniques can detect a larger range than MODIS. The results from the comparison between SPARE-ICE and the independent dataset MODIS further conform that SPARE-ICE is a reliable product.

SPARE-ICE shows its value in model evaluation via the comparison with ECHAM. Their Nash-Sutcliffe efficiencies imply that ECHAM is more accurate than

observation in some regions like central Asia and south Indian Ocean. In the EOF analysis, they also depict similar spatial and temporal EOF patterns.

Overall, it is adequate to conclude that SPARE-ICE is a reliable and usable product from the rational results of this study. It is promising for use in climate research.

# References

Albiñana, A. P., Battles, D., Monteiro, D., Lambeck, R. W., Alemán, R. M., & Jackson, C. (2007, September). The performance of the AVHRR, HIRS, and AMSU-A instruments on board Metop-A. In Optical Engineering and Applications (pp. 667818-667818). International Society for Optics and Photonics.

Assembly of Mathematical and Physical Sciences (US). (1979). Carbon Dioxide and Climate: A Scientific Assessment. National Academy of Sciences.

Buehler, S. A., Jimenez, C., Evans, K. F., Eriksson, P., Rydberg, B., Heymsfield, A. J., Stubenrauch, C. J., Lohmann, U., Emde, C., John, V. O., & Davis, C. P. (2007). A concept for a satellite mission to measure cloud ice water path, ice particle size, and cloud altitude. Quarterly Journal of the Royal Meteorological Society, 133 (S2), 109-128.

Center, E. M. (2010). NCEP Climate Forecast System Reanalysis (CFSR) selected hourly time-series products, January 1979 to December 2010. Research Data Archive at the National Center for Atmospheric Research, Computational and Information Systems Laboratory. [Available online at http://rda. ucar. edu/datasets/ds093. 1.].

Cess, R. D., Zhang, M. H., Minnis, P., Corsetti, L., Dutton, E. G., Forgan, B. W., Garber, D. P., Gates, W. L., Hack, J. J., Harrison, E. F., Jing, X., Kiehl, J. T., Long. C. N., Morcrette, J.-J., Potter, G. L., Ramanathan, V., Subasilar, B., Whitlock, C. H., Young, D. F., & Zhou, Y. (1995). Absorption of solar radiation by clouds: Observations versus models. Science, 267(5197), 496-499.

Chen, R., Ersi, K., Yang, J., Lu, S., & Zhao, W. (2004). Validation of five global radiation models with measured daily data in China. Energy Conversion and Management, 45(11), 1759-1769.

Eliasson, S. (2011). Ice clouds in satellite observations and climate models. Tech. rep.

Eliasson, S., Buehler, S. A., Milz, M., Eriksson, P., & John, V. O. (2011). Assessing observed and modelled spatial distributions of ice water path using satellite data. Atmospheric Chemistry and Physics, 11(1), 375-391.

Eliasson, S., Holl, G., Buehler, S. A., Kuhn, T., Stengel, M., Iturbide-Sanchez, F., & Johnston, M. (2013). Systematic and random errors between collocated satellite ice water path observations. Journal of Geophysical Research: Atmospheres, 118(6), 2629-2642.

Frankignoul, C., Duchene, C., & Cane, M. A. (1989). A statistical approach to testing equatorial ocean models with observed data. Journal of Physical Oceanography, 19(9), 1191-1207.

Heymsfield, A. J. (1977). Precipitation development in stratiform ice clouds: A microphysical and dynamical study. Journal of the Atmospheric Sciences, 34(2), 367-381.

Holl, G. (2011). Microwave and infrared remote sensing of ice clouds: measurements and radiative transfer simulations. Tech. rep., Lulea University of Technology, Department of Computer Science, Electrical and Space Engineering Division of Space Technology, licentiate thesis, ISBN 978-91-7439-374-3, ISSN 1402-1757.

Holl, G., Buehler, S. A., Rydberg, B., & Jimenez, C. (2010). Collocating satellite-based radar and radiometer measurements–methodology and usage examples. Atmospheric Measurement Techniques, 3(3), 693-708.

Holl, G., Eliasson, S., Mendrok, J., & Buehler, S. A. (2014). SPARE‐ICE: Synergistic ice water path from passive operational sensors. Journal of Geophysical Research: Atmospheres, 119(3), 1504-1523.

Houze Jr, R. A. (2014). Cloud dynamics (Vol. 104). Academic press.

Huang, J., Minnis, P., Lin, B., Wang, T., Yi, Y., Hu, Y., Sun-Mack, S., & Ayers, K. (2006). Possible influences of Asian dust aerosols on cloud properties and radiative forcing observed from MODIS and CERES. Geophysical Research Letters, 33(6).

Huang, X., Farrara, J., Leroy, S. S., Yung, Y. L., & Goody, R. M. (2002). Cloud variability as revealed in outgoing infrared spectra: Comparing model to observation with spectral EOF analysis. Geophysical Research Letters, 29(8), 111-1.

John, V. O., Holl, G., Buehler, S. A., Candy, B., Saunders, R. W., & Parker, D. E. (2012). Understanding intersatellite biases of microwave humidity sounders using global simultaneous nadir overpasses. Journal of Geophysical Research: Atmospheres (1984–2012), 117(D2).

Krakauer, N. Y., Pradhanang, S. M., Lakhankar, T., & Jha, A. K. (2013). Evaluating satellite products for precipitation estimation in mountain regions: A case study for Nepal. Remote Sensing, 5(8), 4107-4123.

Krasnopolsky, V. M. (2007). Neural network emulations for complex multidimensional geophysical mappings: Applications of neural network techniques to atmospheric and oceanic satellite retrievals and numerical modeling. Reviews of Geophysics, 45(3).

Kleespies, T. J., & Watts, P. (2006). Comparison of simulated radiances, Jacobians and linear error analysis for the Microwave Humidity Sounder and the Advanced Microwave Sounding Unit‐B. Quarterly Journal of the Royal Meteorological Society, 132(621C), 3001-3010.

Lary, D. J., & Lait, L. (2006). Using probability distribution functions for satellite

validation. Geoscience and Remote Sensing, IEEE Transactions on, 44(5), 1359-1366.

Li, J. L., Waliser, D. E., Chen, W. T., Guan, B., Kubar, T., Stephens, G., Ma, H.-Y., Deng, M., Donner, L., Seman, C., & Horowitz, L. (2012). An observationally based evaluation of cloud ice water in CMIP3 and CMIP5 GCMs and contemporary reanalyses using contemporary satellite data. Journal of Geophysical Research: Atmospheres (1984–2012),117(D16).

Lorenz, E. N. (1956). Empirical orthogonal functions and statistical weather prediction.

Mace, G., & Deng, M. (2011). Level 2 CloudSat-CALIPSO combined ice cloud property retrieval product process description document. NASA CloudSat Project Rep.

Nakajima, T., & King, M. D. (1990). Determination of the optical thickness and effective particle radius of clouds from reflected solar radiation measurements. Part I: Theory. Journal of the atmospheric sciences, 47(15), 1878-1893.

Nash, J., & Sutcliffe, J. V. (1970). River flow forecasting through conceptual models part I-A discussion of principles. Journal of hydrology, 10(3), 282-290.

Price, J. C. (1984). Land surface temperature measurements from the split window channels of the NOAA 7 Advanced Very High Resolution Radiometer.Journal of Geophysical Research: Atmospheres (1984–2012), 89(D5), 7231-7237.

Sassen, K., & Wang, Z. (2008). Classifying clouds around the globe with the CloudSat radar: 1‐year of results. Geophysical Research Letters, 35(4).

Schiffer, R. A., & Rossow, W. B. (1983). The International Satellite Cloud Climatology Project(ISCCP)- The first project of the World Climate Research Programme. American Meteorological Society, Bulletin, 64, 779-784.

Schneider, M., & Hase, F. (2011). Optimal estimation of tropospheric H 2 O and δD with IASI/METOP. Atmospheric Chemistry and Physics, 11(21), 11207-11220.

Solomon, S. (Ed.). (2007). Climate change 2007-the physical science basis: Working group I contribution to the fourth assessment report of the IPCC (Vol. 4). Cambridge University Press.

Stevens, B., Giorgetta, M., Esch, M., Mauritsen, T., Crueger, T., Rast, S., Salzmann, M. Schmidt, H., Bader, J., Block, K., Brokopf, R., Fast, I., Kinne, S., Kornblueh, L., Lohmann, U., Pincus, R., Reichler, T., & Roeckner, E. (2013). Atmospheric component of the MPI‐M Earth System Model: ECHAM6. Journal of Advances in Modeling Earth Systems, 5(2), 146-172.

Waliser, D. E., Li, J. L. F., Woods, C. P., Austin, R. T., Bacmeister, J., Chern, J., Genio, A. D., Jiang, J. H., Kuang, Z., Meng, H., Minnis, P., Platnick, S., Rossow, W. B., Stephens, G. L., Sun-Mack, S., Tao, W.-K., Tompkins, A. M., Vane, D. G., Walker, C. & Wu, D. (2009). Cloud ice:

A climate model challenge with signs and expectations of progress. Journal of Geophysical Research: Atmospheres (1984–2012), 114(D8).

Wallace, J. M., & Hobbs, P. V. (2006). Atmospheric science: an introductory survey (Vol. 92). Academic press.

Wu, M. L. C. (1987). Determination of cloud ice water content and geometrical thickness using microwave and infrared radiometric measurements. Journal of climate and applied meteorology, 26(8), 878-884.

Winker, D. M., Vaughan, M. A., Omar, A., Hu, Y., Powell, K. A., Liu, Z., Hunt, W., & Young, S. A. (2009). Overview of the CALIPSO mission and CALIOP data processing algorithms. Journal of Atmospheric and Oceanic Technology,26(11), 2310-2323.

Yang, W., Shabanov, N. V., Huang, D., Wang, W., Dickinson, R. E., Nemani, R. R., Knyazikhin, Y., & Myneni, R. B. (2006). Analysis of leaf area index products from combination of MODIS Terra and Aqua data. Remote Sensing of Environment,104(3), 297-312.

# Acknowledgments

Many climate researches are indispensable to the accurate data from observation. The pursuit of precision makes the subject of Satellite Remote Sensing so significant in Climate Research. One year ago I was given the opportunity to work at the Applied Meteorology group of Meteorology Institute, University Hamburg and I feel very fortunate to make a small contribution to the scientific community. Therefore it is about time for me to thank all those who played a major part in the finalization of this master thesis.

For offering this topic to me, his great support and his constructive advice, I would like to thank my supervisor Prof. Dr. Stefan Bühler. Also, I am very thankful to my second supervisor Dr. Verena Grützun, for the aid and especially for the thorough review of my work.

In the respect of scientific writing, Prof. Dr. Aike Beckmann helped me a lot by giving me lectures of “Scientific Writing”, and my friends Simon Stoll and Francis Smith corrected some language mistakes for me.

My colleagues at the Applied Meteorology group created a very positive working atmosphere, that lead to productive and helpful discussions and suggestions. I would also like to mention my classmates, who were great company throughout this program of study.

From the course “Climate and Satellite Data Analysis” given by Prof. Dr. Lars Kaleschke, I learned the Nash-Sutcliffe efficiency as a method for model evaluation. The application of EOF analysis was inspired by Dr. Lars Klüser, one of my colleagues at DLR, during my internship.

I acknowledge the World Climate Research Programme's Working Group on Coupled Modeling, which is responsible for CMIP, and I thank the climate modeling groups Max Planck Institute for Meteorology for producing and making available their model output. For CMIP the U.S. Department of Energy's Program for Climate Model Diagnosis and Intercomparison provided coordinating support and led development of software infrastructure in partnership with the Global Organization for Earth System Science Portals.

Finally I want to thank my parents from the bottom of my heart for being my parents.

# Appendix

## Abbreviation

| | |
|---|---|
| AMSU-B | Advanced Microwave Sounding Unit B |
| AVHRR | Advanced Very High Resolution Radiometer |
| CALIOP | Cloud-Aerosol Lidar with Orthogonal Polarization |
| CALIPSO | Cloud-Aerosol Lidar and Infrared Pathfinder Satellite Observation |
| CFSR | Climate Forecast System Reanalysis |
| CMSAF | Satellite Application Facility on Climate Monitoring |
| CPR | Cloud Profiling Radar |
| DARDAR | Active combined raDAR-liDAR product |
| EOF | Empirical Orthogonal Function |
| FE | Fractional Error |
| IR | Infrared |
| IWC | Ice Water Content |
| IWP | Ice Water Path |
| LWC | Liquid Water Content |
| MFE | Median of Fractional Error |
| MHS | Microwave Humidity Sounder |
| MODIS | Moderate Resolution Imaging Spectroradiometer |
| MSPPS | Microwave Surface and Precipitation Products System |
| MW | Microwave |
| NOAA | National Oceanic and Atmospheric Administration |
| PC | Principle Component |

| | |
|---|---|
| PDF | Probability Density Function |
| PMW | Passive Microwave |
| POES | Polar Orbiting Environment Satellites |
| RMSD | Root-Mean-Square Difference |
| SPARE-ICE | Synergistic Passive Atmospheric Retrieval Experiment-ICE |
| SRBS | Solar Reflectance Bispectrum |
| STD | Standard Deviation |
| VIS | Visible light |

# Declaration of Academic Integrity

I hereby truthfully and solemnly declare on oath that I have carried out this thesis entirely myself and without the help of any third party and that all literal quotations and other authors' ide- as have completely been accounted for. This thesis contains no material that has been sub- mitted previously, in whole or in part, for the award of any other academic degree or diplo- ma. The submitted printed and electronic versions are identical.

Hiermit erkläre ich an Eides Statt, dass ich die vorliegende Arbeit selbstständig und ohne fremde Hilfe verfasst, keine anderen als die angegebenen Quellen und Hilfsmittel verwendet habe, die Arbeit vorher nicht in einem anderen Prüfungsverfahren eingereicht habe und dass die gedruckte Version mit der auf dem elektronischen Speichermedium identisch ist. Alle Stellen, die wörtlich oder sinngemäß aus Veröffentlichungen entnommen wurden, sind als solche kenntlich gemacht.

Hamburg, 12 Dec. 2015, Shengyin Li

Signature